

Forschungszentrum Karlsruhe
in der Helmholtz-Gemeinschaft

Wissenschaftliche Berichte

FZKA 6853
SAM-COLOSS-P057

Analytical Support for the
B₄C Control Rod Test QUENCH-09

Ch. Homann, W. Hering

Institut für Reaktorsicherheit

Forschungszentrum Karlsruhe GmbH, Karlsruhe
2003

Impressum der Print-Ausgabe:

**Als Manuskript gedruckt
Für diesen Bericht behalten wir uns alle Rechte vor**

**Forschungszentrum Karlsruhe GmbH
Postfach 3640, 76021 Karlsruhe**

**Mitglied der Hermann von Helmholtz-Gemeinschaft
Deutscher Forschungszentren (HGF)**

ISSN 0947-8620

Abstract

Degradation of B₄C absorber rods during a beyond design accident in a nuclear power reactor may be a safety concern. Among others, the integral test QUENCH-09 is performed in the FZK QUENCH facility and supported by analytical work within the Euratom Fifth Framework Programme on Nuclear Fission Safety to get a more profound database. This analytical support for the preparation of the test relied on QUENCH-07 post-test analysis, but the inclusion of a test phase with a small steam mass flow, not investigated in any QUENCH test before, resulted in some work for pre-test calculations to guarantee the safety of the facility, to derive the test protocol and to choose an appropriate instrumentation. Several institutions shared in this work with different computer code systems, as used for nuclear reactor safety analyses. All pre-test calculations showed the same trends. Especially the high temperatures and hence the small safety margin for the facility were a concern. Post-test analysis showed some open problems, which cannot be solved in a short time. In this report, only FZK contributions are presented.

The test QUENCH-09 and the related computational support by the engaged institutions were co-financed by the European Community under the Euratom Fifth Framework Programme on Nuclear Fission Safety 1998 – 2002 (COLOSS Project, contract No. FIKS-CT-1999-00002).

Zusammenfassung

Analytische Unterstützung für das B₄C Kontrollstab-Experiment QUENCH-09

Das Versagen von B₄C Absorberstäben bei einem auslegungsüberschreitenden Unfall in einem Kernkraftwerk kann von Bedeutung für die Einhaltung der Sicherheitsrichtlinien sein. Um eine bessere Datenbasis zu bekommen, wird im Rahmen des 5. Rahmenprogramms der Euratom zur Sicherheit der Kernspaltung unter anderem der Integraltest QUENCH-09 in der QUENCH-Anlage des FZK durchgeführt und durch analytische Arbeiten unterstützt. Diese analytische Unterstützung für die Testvorbereitung beruhte auf den Nachrechnungen zu QUENCH-07, aber der Einschluss einer Testphase mit geringem Dampfdurchsatz, der noch nie in einem QUENCH-Versuch untersucht wurde, bedeutete einige Arbeit für die Vorausrechnungen, um die Sicherheit der Anlage zu garantieren, den Versuchsablauf und eine geeignete Instrumentierung festzulegen. An dieser Arbeit haben sich mehrere Forschungseinrichtungen mit unterschiedlichen Rechenprogrammen beteiligt, die für Sicherheitsanalysen von Kernreaktoren benutzt werden. Vor allem die hohen Temperaturen und der dadurch bedingte geringe Sicherheitsspielraum für die Anlage waren von Interesse. Nachrechnungen zeigten offene Probleme, die sich nicht in kurzer Zeit lösen lassen. In diesem Bericht werden nur Beiträge des FZK dargestellt.

Der Versuch QUENCH-09 und die zugehörige Unterstützung durch Rechnungen durch die beteiligten Einrichtungen wurden teilweise im 5. Rahmenprogramm der Euroatom zur Sicherheit der Kernspaltung 1998 – 2002 (Projekt COLOSS, Vertragsnummer FIKS-CT-1999-00002) durch die Europäische Union finanziert.

Table of Contents

Abstract	i
Zusammenfassung	ii
Table of Contents	iii
List of Figures	iii
1 Introduction.....	1
2 Experimental Basis.....	2
2.1 QUENCH Facility.....	2
2.2 Test Protocol	3
3 Calculations.....	3
3.1 Modelling of the QUENCH Facility	4
3.2 Pre-Test Calculations	5
3.3 Post-Test Calculations	6
4 First analysis of B ₄ C control rod failure.....	8
5 Conclusions.....	10
6 Acknowledgement	10
7 Literature	11
Figures	12

List of Figures

Fig. 1: Main flow paths in the QUENCH facility	12
Fig. 2: Cross section of the test section for QUENCH-09	13
Fig. 3: Test protocol for QUENCH-09.....	14
Fig. 4: Modelling of the QUENCH facility with SCDAP/RELAP5	15
Fig. 5: Survey of pre-test calculations with 16f model	16
Fig. 6: Survey of pre-test calculations with 32f model	17
Fig. 7: Temperatures as a function of time (pre-test calculations)	18
Fig. 8: Selected variables as a function of time (pre-test calculations)	19
Fig. 9: Axial profiles of selected variables, part 1 (pre-test calculations).....	20
Fig. 10: Axial profiles of selected variables, part 2 (pre-test calculations).....	21
Fig. 11: Axial profiles of selected variables, part 3 (pre-test calculations).....	22
Fig. 12: Conduct of test QUENCH-09	23
Fig. 13: Selected variables as a function of time (post-test calculation).....	24
Fig. 14: Axial temperature profiles at three different times (post-test calculation).....	25
Fig. 15: Measured and calculated fluid temperatures (post-test calculation)	26
Fig. 16: Measured and calculated fluid temperatures (post-test calculation, cool-down).....	27
Fig. 17: Selected variables as a function of time (parameter study)	28
Fig. 18: Axial temperature profiles (manufacturer's data for shroud insulation)	29
Fig. 19: Axial temperature profiles in the second transient (part 1).....	30
Fig. 20: Axial temperature profiles in the second transient (part 2).....	31
Fig. 21: Selected variables as a function of time (parameter study, cool-down phase)	32
Fig. 22: Selected variables as a function of time (oxidation correlation)	33
Fig. 23: Selected variables as a function of time (oxidation correlation, cool-down phase) ...	34

1 Introduction

Though in a nuclear power reactor the number of absorber elements is small (about 4 %) in comparison to the number of fuel rods, the effects of the degradation of absorber elements in an accident cannot be neglected because of their relatively low melting temperature. During their degradation droplets of hot material are deposited on the cladding of the surrounding fuel rods, and the resulting compounds influence the physical and chemical behaviour of the fuel rods, e.g. by lowering melting points. Besides the formation of gaseous oxidation products of B_4C , especially of CH_4 , is of interest for safety considerations for the following reason. When the steam mass flow in the core is small enough, CH_4 may be formed mainly in colder parts of the primary circuit and in the containment; of course, a certain steam mass flow is needed to oxidise B_4C . When fuel rods also fail and fission products are released, CH_4 may be transformed into volatile organic iodine compounds. These compounds cannot be retained appropriately by filters, and hence are a safety concern when released into the environment.

Because of this importance for reactor safety considerations the impact of B_4C absorber rod degradation during a postulated accident in a nuclear power reactor is dealt in the COLOSS Project, which is part of the Euratom Fifth Framework Programme on Nuclear Fission Safety (5th FWP), launched by the European Community. Among others three integral experiments and related pre- and post-test calculations with large severe accident code systems, currently used for safety analyses in nuclear power reactors, are supported and co-financed by the European Community. For VVER-1000 reactor conditions this item is addressed in the CODEX-B4C experiment, performed in the CODEX facility at AEKI /1/, and for Western type reactors in tests QUENCH-07 /2/ and QUENCH-09 /3/, both performed in the QUENCH facility at FZK. In this report, however, only test QUENCH-09 will be addressed.

In detail, test QUENCH-09 is to fulfil three aims. Firstly it should provide experimental data on degradation of B_4C control rods, its impact on surrounding fuel rods, and the production of gas (in particular H_2 and CH_4) before and during reflood in conditions as representative as possible of commercial 1300 MW Pressurized and Boiling Water Reactors (PWR and BWR). Secondly it should provide a useful database for the preparation of the future PHEBUS FPT3 in-pile experiment /4/, and thirdly to give information for other test conditions than those of test QUENCH-07 to enlarge the database as much as possible. For the last reason the conduct of test QUENCH-09 was based on that of QUENCH-07, but with differences after the plateau phase, i.e. after bundle temperature has been kept at a maximum of more than 1700 K for some time. Above all a test phase with low steam mass flow is envisaged. Because of this modification, the two QUENCH tests with a B_4C absorber rod shed light on a large range of important reactor accident scenarios: steam starved conditions may occur in a large break LOCA (Loss of Coolant Accident), while steam excess is likely in a LOOP (Loss Of Off-site Power) scenario.

The projected test differed in more than one aspect from QUENCH tests before QUENCH-07, and it differed essentially from QUENCH-07 by the inclusion of a phase with only low steam mass flow. As for the previous test /5/ it was therefore thought prudent to rely on more than one institution and on more than one code system to prepare the test and to determine the test conduct. The aims of these calculations were twofold. They should give a sufficient confidence that the integrity of the QUENCH facility would be maintained in the test and they should help to optimize the test conduct, so that as much benefit as possible could be drawn from the experiment.

The following institutions participated in pre- and post-test calculations and performed independent calculations for test QUENCH-09, (in alphabetic order of their tokens) Ente per le Nuove Tecnologie, l'Energia e l'Ambiente (ENEA) at Bologna, Italy, with ICARE/CATHARE, Forschungszentrum Karlsruhe (FZK), Germany, with SCDAP/RELAP5, Institut für Kernenergetik und Energiesysteme (IKE) at Stuttgart University, Germany, with ATHLET-CD, Paul Scherrer Institut (PSI), Villigen, Switzerland, with SCDAP/RELAP5, and Universidad Politécnica de Madrid (UPM), Madrid, Spain, with ICARE2. They helped identifying and solving problems associated with the planning and performing of this test, and many fruitful discussions in the various COLOSS meetings and elsewhere. Especially, between PSI and FZK a close cooperation had already been initiated for the preparation of QUENCH-07, because in both institutions SCDAP/RELAP5 (S/R5) mod 3.2 /6/ was used. In that context, FZK delivered FZK programme extensions /7/ and a current input deck to PSI. In fact, however, the two programme versions were intentionally somewhat, but not seriously, different /5/.

In this report only FZK work for pre- and post-test analysis of test QUENCH-09 is documented, showing crucial points in the preparation of the test and the status of the work with open questions for further analysis. Contributions by the other participants will be documented in separate reports. As an outlook for general modelling of B₄C absorber rod failure, a comparison of respective phenomena, observed in QUENCH-07 and QUENCH-09 and the consequences as well in these test as well as for reactor conditions is added.

2 Experimental Basis

2.1 QUENCH Facility

In the following a short description of various aspects of the QUENCH facility is given. More details are documented in /2/ and /8/. The QUENCH facility (Fig. 1) consists of the test section as its main part and a number of external devices. The test section consists of a bundle with 21 rods (Fig. 2). Their arrangement and their cladding are typical for commercial Western type PWRs. In test QUENCH-09 the central rod is a control rod, essentially as used in Western type PWRs with a B₄C absorber rod; the absorber rod design is identical to that for the projected PHEBUS test FPT3. The other 20 rods are fuel rod simulators with annular ZrO₂ pellets, heated electrically over a length of 1.024 m; the tungsten heaters are connected to a combination of molybdenum and copper electrodes at both ends. Electrical power supply is independent for the eight inner and the twelve outer rod simulators. The four Zircaloy corner rods are intended to improve thermal-hydraulic conditions in the bundle; in addition, they are used for instrumentation. One of them may be removed during the test to analyze the axial profile of the oxide layer thickness, formed up to that time. The bundle is contained in a Zircaloy shroud and insulated by ZrO₂ fibre material. The whole set-up is enclosed in a steel containment.

A mixture of steam and argon enters the bundle from the bottom; the fluid, i.e. steam, argon, hydrogen and other products formed or released in the bundle, leaves the bundle at its top to enter the off-gas pipe. In the cooling jacket, there is a counter-current water flow in the upper electrode zone and a counter-current argon flow in the heated and the lower electrode zone.

The test section up to and including the outer cooling jacket is equipped with nearly 90 thermocouples at 17 axial locations in the heated and in both electrode zones. Fluid composition is

mainly analyzed by two quadrupole mass spectrometers in the off-gas pipe downstream of the bundle.

2.2 Test Protocol

After discussions in several COLOSS meetings /9/ and /10/ about the optimal test conduct, the following test protocol was set up (Fig. 3). As usual in QUENCH tests, the experiment begins with a stabilisation phase with a constant maximum bundle temperature of about 800 K. In this phase, checks are performed to verify the correct working of the various systems. Temperatures are already at an elevated level, but low enough to avoid premature oxidation. A power transient as in QUENCH-07 is applied afterwards (first transient) to reach a maximum bundle temperature of more than 1700 K. This temperature is kept for some time (plateau phase). Steam mass flow rate is 3 g/s from the beginning of the test up to the end of the plateau phase. For the subsequent temperature transient (second transient) electrical power input is kept constant (dashed line in Fig. 3, bottom), and steam mass flow is reduced to 0.3 g/s. This value is close to that which is selected for PHEBUS FPT3 and accounts for the different oxidising surfaces in the two facilities. The second transient is performed differently to QUENCH-07, where electrical power (solid line in Fig. 3, bottom) was increased and the steam mass flow rate was kept constant at 3 g/s. Cool-down begins when temperature criteria are met as in QUENCH-07. It is performed with a steam mass flow rate of 50 g/s instead of 15 g/s as in QUENCH-07, intended to conserve the status of the bundle at the end of the transient.

If no reaction products from the degradation of the absorber rod are detected, the plateau phase before the second transient should last 5 minutes; otherwise, the plateau phase should last 15 minutes to facilitate the detection of the reaction products as in QUENCH-07. The decision about the second transient is in contrast to what was decided for QUENCH-07 /2/, /5/. In that test, low steam flow conditions during the plateau phase were not investigated because of the concern to damage the facility. For the transient before cool-down, low steam flow conditions were avoided, because time for measurements was predicted to be smaller than for high steam flow conditions /5/. QUENCH-09, however, is the second experiment with a B₄C absorber and hence can rely upon experience for QUENCH-07, and firstly low steam flow conditions are relevant for reactor safety analyses in general, and secondly such test conditions are closer to the projected PHEBUS FPT3 experiment.

In the discussions about QUENCH-09, the risk for the integrity of the facility was supposed to be tolerable, because the test conduct can easily be changed during the test, if problems occur. Nevertheless, the experimental team has to be rather careful, when the test is performed, because the facility reacts rather sensitively to changes of the test parameters, when the steam mass flow is small.

3 Calculations

From the very beginning of the project, QUENCH activities have been supported by calculations with SCDAP/RELAP5 (S/R5) /6/ to define experimental parameters of the QUENCH experiments and to interpret the experimental results after the test. For the calculations presented here, the in-house version of S/R5 mod 3.2 has been used; the new code version, mod 3.3, is still inoperable; severe code errors have been reported to the code developers, but user support by the code developer is not any longer available. Among others, the current in-house version contains

an improved model for heat transfer in the transition boiling region /11/, an adaptation of the CORA heater rod model to the conditions of the QUENCH facility, and the material property data for ZrO_2 instead of those for UO_2 to model the pellets /7/.

The various calculations also rely on the experience gained from the calculations done for the previous quench tests. Especially the adjustment of the electrical resistance of the circuit outside the electrical heater rods and the adjustment of the thermal conductivity of the shroud insulation, both based on calculations for test QUENCH-01 /12/, were kept.

3.1 Modelling of the QUENCH Facility

The modelling of the QUENCH facility with S/R5 is the same for all tests that are investigated. In the radial direction, the whole facility including the containment is modelled (Fig. 4), because the radial heat losses out of the bundle depend ultimately on the ambient room temperature. This modelling is mandatory for all work performed before experimental data are available, and it is desirable for all post-test analyses, because the calculated data are more detailed than the experimental ones.

The central rod, the two rings of rods to be heated independently, the four Zircaloy corner rods, the inner and outer cooling jacket, and the containment are modelled as SCDAP components. Two-dimensional heat conduction within the structures and radiation between adjacent structures are taken into account. The temperature at the end of the rods is set to 300 K. In the first pre-test calculations, the central rod is modelled as an unheated fuel rod, because the original SCDAP absorber models are rather poor or even inappropriate. In parallel, the SCDAP model for the PWR control rod component was extended; now it includes the correct B_4C material property data. B_4C oxidation is not yet taken into account, because before the development of a respective code model further interpretation of separate effect tests at FZK is necessary. In all post-test calculations, the new model is therefore used for the central rod. The corner rods are modelled as fuel rods. For the electrical resistance of the circuit outside the electrical heater rods the same value of 4.2 m Ω per rod is used as for test QUENCH-01 /12/. The ZrO_2 fibre insulation is modelled to end at the upper end of the heated zone. With this exception, all structures must be modelled to have the same length because of limitations in the code. Therefore, the upper and lower head cannot be modelled in all details.

The bundle flow and the gas atmospheres outside the outer cooling jacket, i.e. in the containment and the laboratory, are represented by a single channel each. The gas atmospheres outside the outer cooling jacket are assumed stagnant, thus neglecting natural convection in these regions. Because of restrictions in the code, where only a limited number of materials can be specified, these atmospheres are modelled to consist of argon.

The off-gas pipe is taken into account with its whole length of 3 m, including the orifice at the position where the gas sample for the mass spectrometer is taken and the orifice at the outlet of the off-gas pipe to simulate correctly the pressure boundary conditions during reflood phase. The mass flows in the off-gas pipe and the adjacent cooling jacket are modelled to be one-dimensional, the structures are modelled as RELAP heat structures, thus taking into account radial heat transfer within the structures.

For most calculations, the region of the heated part is axially modelled with ten 0.1 m long mesh cells. In the lower and upper electrode zones 0.45 and 0.6 m, respectively, of the test section are considered, each by three mesh cells. For the lowermost node in the lower electrode zone copper as electrode material is assumed and molybdenum elsewhere. In addition to this 16 nodes

facility (16f) model a 32 nodes facility (32f) model is available, where the whole facility is modelled as in the 16f model, but all axial mesh lengths as well in the heated zone as well as the electrode zones are halved. Again, copper is assumed as electrode material in the lowermost zone of the lower electrode zone and molybdenum elsewhere. Besides, the radial discretization of the fuel simulator rods has been refined. Furthermore, a 32 nodes bundle (32b) model has been created as a fast running approximate solution, with all axial mesh lengths as in the 32f model /8/. However, only one SCDAP component is used to simulate all heated rods, and the corner rods are not modelled. The facility outside the cooling flows is not considered. Instead, the flow area for the argon cooling flow is changed artificially to result in realistic radial heat losses out of the bundle. A 16 nodes bundle (16b) model may easily be created, but is not used actually.

3.2 Pre-Test Calculations

Since the first phases of test QUENCH-09 are planned to be as in test QUENCH-07, the physical initial and boundary conditions simulated in the pre-test calculations are taken from first post-test calculations for that test /5/. These post-test calculations gave, however, too large deviations between calculated and measured temperatures and hydrogen production rates, even before the second transient begins in QUENCH-09. The differences are mainly in the hot zone and too large to be acceptable for reliable pre-test calculations for QUENCH-09, because the hot zone is the most important and the most critical issue for the test conduct. As a first step, the electrical power has been modified with respect to QUENCH-07 experimental data so that measured temperatures are sufficiently well met in the calculation for the phases up to and including the temperature plateau, above all in the hot zone. Representative results, obtained with the 16f model, are given in Fig. 5. Experimental values from QUENCH-07 are included for comparison in this and in the following figures. Computational run q09v01 corresponds to QUENCH-07 post-test calculation up to the end of the temperature plateau. Electrical power refers to the value as measured in the tests and hence contains a portion released in the circuit outside the computational domain. It gives also an impression of the sensitivity of the facility, when experimental parameters are changed. This is due to the high bundle temperature and, furthermore, the smaller convective heat removal, when the steam mass flow rate is decreased. These findings also show that the reaction time for operators is limited.

These analyses were continued with the 32f model for more detailed results. An overview similar to Fig. 5 is given in Fig. 6. Beginning with run q09w07 the current absorber model is used for the central rod. In accordance with the work for QUENCH-07 /5/ both figures show the relatively small safety margin for the facility during the test conduct.

Representative results (run q09w08) are given in Fig. 7 to Fig. 11. In the plots for power “input” means total electrical power input as measured, and “elec” means that part of the electrical power, which is released in the bundle. The difference between these two powers is released outside the computational domain, e.g. in the sliding contacts or the wires leading to the power supply. “oxid” refers to chemical power release.

The deviations to measured temperatures in the lower part of the bundle are not crucial for the planning of the test because of the relatively low temperatures. The time dependant results as well as the axial profiles show that during the second transient practically the whole steam supply is consumed in the bundle as it is intended. The peculiar oxide layer profile for the absorber rod may be attributed to rod degradation.

During the second transient, the axial temperature profile becomes broader. The maximum of hydrogen production rate shifts markedly to lower axial elevations. The maxima of temperature and oxide layer thickness also shift into that direction, but much less than hydrogen production rate. Above all the temperature shift is an essential issue for the preparation of the test insofar as to choose appropriate thermocouples. If the temperature maximum shifts substantially to lower parts of the heated zone during the test, high temperature thermocouples are also needed in those parts. This is in contrast to former QUENCH tests and causes some technical problems. In fact, other participants calculated larger shifts of the maximum temperature, eventually even a second maximum in the lower bundle half. A detailed inspection of their results shows, however, that their second transient is longer so that higher temperatures are reached than in QUENCH-07 and larger effects occur mainly at later times than considered in our calculations. Our pre-test calculations for QUENCH-07 suggest that a larger temperature shift and a second maximum in the bundle centre may be expected for a longer transient. During steam cool-down, some limited temperature escalation is predicted to occur due to local shattering of the oxide layer, but problems for the test conduct are not identified.

Comparison with results for run q09w06, where the central rod is modelled as an unheated fuel pin, shows only small differences. Similarly, the influence of axial discretization is limited, as can be seen by comparing the results with that of run q09v05, which refers to the coarse axial discretization with the 16f model. For that calculation, a longer second transient has been assumed. The figures also demonstrate the change of local electrical power input due to the well-known positive feedback for electrically heated rods. The electrical resistance increases with temperature and so does the local electrical power. This in turn increases temperature and hence local power release. This effect is still enhanced by oxidation, which increases temperature further.

3.3 Post-Test Calculations

Post-test calculations are based on the real test conduct as shown in Fig. 12 with the same modelling as for the pre-test calculations. Results are given in Fig. 13 as a function of time. Label "16 nodes" refers to the 16f model. In the first transient, calculated temperatures are underestimated at the top of the heated zone (axial level 13), and in the plateau phase temperatures are calculated to increase further. Before steam mass flow reduction, hydrogen production is hence underestimated. The slow measured decrease of hydrogen production after steam mass flow reduction may come from hydrogen accumulated e.g. in the upper plenum, from where it diffuses only slowly into the main stream.

Values for measured temperatures up to 2633 s are mainly between calculated rod surface and bundle fluid temperature as can be expected for thermocouples mounted on the outer clad surface (Fig. 14). Differences occur around the upper end of the heated zone; especially the escalation at the upper end of the heated zone is not calculated. Previous experimental work showed that temperature escalations detected by bundle thermocouples at levels 11 and 12 (elevations 0.75 and 0.85 m) and shroud thermocouples in the upper electrode zone may be questionable, when an escalation occurs at level 13. Because of this finding, deviations between measured and calculated temperatures at high temperatures at 2633 s and later are smaller than they appear in Fig. 14. For 3315 s, the axial temperature profile in the heated zone in the bundle is overestimated, but it is calculated to be rather flat in the upper half of the heated section, and the maximum is shifted somewhat to the bundle centre. The more reliable thermocouples suggest that the temperature profile is indeed rather flat in that region.

Fig. 13 and Fig. 14 also show that there is no significant difference between the coarse and the fine axial discretization of the facility except near the bundle exit and furthermore near the upper end of the heated zone during cool-down. This result is in contrast to that for QUENCH-07 /5/; it may depend on details of the particular test conduct; therefore, it cannot be generalized.

Fluid temperatures, measured at more axial levels than in previous tests, compare quite well with measured ones except at level 6 (Fig. 15). At that level and before cool-down the reading of TFS 2/6, which should be representative of fluid temperature, is close to the value of TFS 5/6, which should be representative of clad surface temperature. Only during the cool-down phase, TFS 2/6 becomes more representative of the fluid temperature (Fig. 16).

For standard calculations the thermal conductivity for the shroud fibre insulation, delivered by the manufacturer, is increased by 40 % to account for the cylindrical geometry which cannot be handled with S/R5 and by another 40 % to meet the experimental data of QUENCH-01, hence in sum by 80 %. This physical parameter was changed to better meet the measured data in the first transient and hence get better-calculated initial conditions for the plateau phase. The parameter study showed that the escalation and the hydrogen production during the heat-up phase can only be calculated using the original manufacturer's data (Fig. 17). The temperature escalation at the time of absorber rod failure agrees quite well with measured temperatures (Fig. 18). However, the results in the following plateau phase cannot be met, and deviations with respect to experimental data are larger than in the first post-test calculation. The calculated time of control rod failure shifts from 2343 s to 2280 s as detected in the experiment.

Since the axial temperature profile during the second transient was a concern in the preparation of the test, measured and calculated data are inspected in more detail. In Fig. 19 and Fig. 20, their values are compared at six different times; in contrast to Fig. 14 the readings of the questionable thermocouples are not included to demonstrate that effect. As a rough estimate for the bundle behaviour, the shroud thermocouples can also be included. At about 2800 s the measured maximum temperature shifts somewhat to the bundle centre, then the profile becomes flatter, and eventually the plateau extends down to elevation 10 (0.65 m). Calculated values overestimate measured ones except in the beginning of the second transient, but the change of the axial profile with time is correctly calculated.

During cool-down the improved local shattering option is used to simulate the extremely high hydrogen production detected in the test, but even so hydrogen production is underestimated (Fig. 21). This result may be expected for these experimental conditions, because except for the beginning of the cool-down phase, where their values depend on the previous phases, temperatures do not depend much on the thermal conductivity of the shroud insulation.

In a further calculation the standard correlations in S/R5 for Zircaloy oxidation (Cathcart and Urbanic-Heidrick for low and high temperatures, respectively) have been replaced by the Leistikow and Prater-Courtright correlations and an interpolation between them according to recommendations made by G. Schanz, FZK, in the COLOSS project. In discussions during COLOSS meetings, it was pointed out, that it is necessary to include a steam supply limitation in the code, when the new oxidation model is applied. For the calculations presented here, the steam limitation model is used, as it is already implemented in the standard version of S/R5 /6/. It is also used for the calculations with the standard oxidation model, presented here. It is based on an analogy of heat and mass transfer and, because dimensionless numbers are used, it should essentially be applicable irrespective of the oxidation model. For QUENCH-09 agreement with experimental data for steam rich conditions (Fig. 22) and during cool-down (Fig. 23), hence in

both temperature regimes, is improved. First results for QUENCH-07, however, give a drastic overestimation of oxidation at high temperatures, but not for plant applications. Consequently, some error checks have still to be done.

A comparison of test QUENCH-07 and QUENCH-09 shows tremendous differences of experimental data after the failure of the absorber rods, though test conditions differ only marginally, if any. The reasons for these differences are not yet clear and probably need some time for a clarification. Consequently, further model development for absorber rod behaviour should not be done before the experimental differences are better understood.

4 First analysis of B₄C control rod failure

For a better understanding of the respective QUENCH tests and as a general basis for code development, the sequence of phenomena, concerning absorber rod degradation in both QUENCH tests, is investigated. This work, as outlined in the following, is based on present knowledge, and further insight is expected, when results of the destructive post-test analyses for QUENCH-09 are available. For a general analysis, it should be kept in mind that in eastern and western LWRs B₄C is used as a powder or as pellets. It is encased in a stainless steel cladding, which is surrounded by a Zircaloy guide tube in PWRs or a canister in BWRs. Therefore, the whole system of B₄C, stainless steel, and zirconium has to be taken into account together with the protective layer of ZrO₂.

To characterize that complex situation, a list of phenomena with increasing temperature is given in Tab. 1, focused on the explanation of the different behaviour observed in QUENCH-07 and QUENCH-09. As can be seen, no difference between the two QUENCH tests is noticeable up to 1550 K for this low-pressure scenario. For reactor scenarios, the pressure history has to be considered which may lead to breach of the stainless steel tubes during primary system depressurization. Since the axial location for the breach may vary due to the scenario and the depressurization time, it will not be mentioned further on.

With the release of liquid materials, composed of B₄C and steel, the absorber rod behaviour and its influence on the environment changed between the two tests. In both cases, the stainless steel tube was penetrated, but in QUENCH-09, no significant amount of reaction products of B₄C degradation was detected before cool-down initiation. This behaviour was quite unexpected. For a better understanding of the test, the following scenario is presently supposed for QUENCH-09.

Since very limited amounts of reaction products were detected [3], it is deduced that no direct steam access to the B₄C was possible at that time and hence the melt remained localized either due to a protective ZrO₂ scale or, more likely, because the melt blocked the breach. Consequently, the time for B₄C-SS interaction is extended and hence the axial length for interaction. Even after exceeding 1700 K, the melting temperature of SS, no release of B₄C oxidation products was detected. It is supposed that sufficiently thick zirconium oxide scales inhibit early absorber material release similarly to observation for AgInCd systems, where the oxide layer encased the metallic liquid that is not released until final heat-up.

In QUENCH-09, the region, where the protective oxide layer is sustained, should be between about 0.55 m and 1.15 m, because in that region temperatures are above 1600 K during the plateau phase. Between 2700 s and 3300 s, measured temperatures exceed 2040 K. This indi-

cates that the α -Zr(O) is liquid, forming a liquid alloy column of app. 0.6 m length, composed of B_4C , SS, and Zr. With the failure of the oxide scale on the guide tube, which occurred during reflood, this liquid is released and oxidized immediately.

Such a scenario would explain the observed rapid increase of CO_2 and CO release, which is favoured by the steam excess during fast cool-down [3]. The ideas mentioned above have to be checked by the results of the destructive post-test analyses. Additionally, other experiments with B_4C absorber rods should be integrated into Tab. 1 to complete and foster the understanding.

Temperature		Phenomena	Significance	Quench		Consequences	Parameters
[K]	[°C]			07	09		
		Clad rupture (depressurization)		No	No	Limited steam access to B_4C	
1250	977	Onset of Zr-SS Interaction (Guide tube - Absorber sheath)	Locally at contact position (hot region)	Y	Y	Initiation of guide tube weakening	Protective: ZrO_2 layer > 50 μ m
1470	1197	Enhanced Zr- B_4C dissolution rate	no	---	---	After failure	no
1473	1200	Liquefaction of the B_4C -SS system	no	Y	Y	Liquid layer of B_4C -SS (kept within ZrO_2 shell)	Limitation: max. 9% wt of B_4C in SS
1550	1277	Perforation of SS and Zr layers by Zr- B_4C /SS interaction	Axial position and size of breach	Y	VL	Release of gases + liquified MeB, increase of breach size, access of steam	Steam concentration, pressure difference
		Lateral relocation/spreading of absorber/steel alloy	Onset of propagation	---	No	Triggers ZrO_2 scale failure in adjacent rods	No large relevance compared to AgInCd - CR
		B_4C Oxidation	Localized	Y	VL	B_4C oxidation limited? release of oxidation products (B_2O_3)	Access of steam through breach
1573	1300	Axially spreading of zone with $T > 1500K$?	Y	No	Increases area for oxidation, compensates the effect of ZrO_2	Electrical and chemical power protection
1723	1450	Melting temperature of SS	no	---	---	Liquid column kept within outer ZrO_2 shell; No longer metallic β -Zry available	no
		Limitation of oxidation?	Chemical thinning of ZrO_2	No	Y	Less protective ZrO_2 layers on fuel rods and absorber rod guide tube	Steam supply
1870	1597	Zr- B_4C reaction rate jumps (app. 2 orders of Mag)	Protective oxide layer inhibits interaction?	?	?	Inhibited by ZrO_2 layer in case of QUENCH-09	wetted surface, mass
2033	1760	Melting temperature of β -Zry		---	---	Enhanced U-Zr-O interaction starts (similar for Zr- ZrO_2)	
2330	2057	Lowest reasonable clad failure temperature (α -Zr(O))	Formation of B_4C -Zr-SS mixture, release possible	Y	Y	Fuel rod: melt release (U-Zr-O), influence of CR behavior?	Limitation: max. 9% wt of B_4C in SS+Zry
?	?	Cool down initiation: high steam supply		---	Y	QUENCH-09: Steam starvation favours uncontrolled temperature escalation	Cool-down in Q-07 faster than in Q-09
		Amount of B_4C reacted		40	>40	% of 1 m bundle fraction (consider only $T > 1500K$!)	

Notes: Some temperatures are lower limits for reaction

Status: based on present knowledge (Jan 2003)

CR: control rod

VL: localized and very limited interaction

Tab. 1: Sequence of phenomena during B_4C degradation in QUENCH tests

5 Conclusions

Computational analysis has been done before and after the test QUENCH-09. The present report demonstrates the status of this work at the end of the COLOSS project in the Fifth Framework Programme on Nuclear Fission Safety, launched by the European Community.

Pre-test calculations are based on post-test analysis of QUENCH-07, but as a quick solution electrical power was modified with respect to test data of QUENCH-07 to improve the agreement between calculated and measured data up to the begin of steam mass flow reduction. The preliminary modelling of the absorber rod does not change results appreciably with respect to former calculations, where an unheated fuel rod is modelled instead. Refinement of the axial mesh length is mainly in the steep gradient in the upper electrode zone and, during cool-down, around the upper end of the heated zone. The axial temperature profile becomes broader with time and maximum of temperature and hydrogen production shift somewhat to lower elevations during the transient. Some limited temperature escalation is predicted to occur during steam cool-down, but no difficulties are predicted in the cool-down phase. The calculations also predict that due to the experimental conditions the QUENCH facility would be rather sensitive to changes of experimental parameters as electrical power input and that the facility might even be damaged during the test.

First post-test calculations showed deviations from experimental data. A parameter study to improve the agreement at the time of the steam mass flow reduction, gave no better results in the subsequent test phase. The recommendations for Zircaloy oxidation correlations gave some improvement, but error checks are not yet finished. Further work is needed, but it also depends on the interpretation of experimental data of this and of separate effect tests.

The sensitivity of the facility, when experimental parameters are changed, and the small safety margin for the given experimental conditions, predicted in the pre-test calculations, was confirmed during the course of the test. This result justifies the large effort, done by several institutions, engaged in the COLOSS project to define an appropriate test conduct for both QUENCH tests with a central B₄C absorber rod.

6 Acknowledgement

The test QUENCH-09 and the related computational support were co-financed by the European Community under the Euratom Fifth Framework Programme on Nuclear Fission Safety 1998 – 2002 (COLOSS Project, contract No. FIKS-CT-1999-00002).

7 Literature

- /1/ Hozer, Z., Nagy, I., Windberg, P., Balasko, M., Matus, L., Prokopiev, O., Czitrovsky, A., Nagy, A., Jani, P.: CODEX-B4C Experimental Data Report, SAM-COLOSS-P020, D17, Budapest, Oct. 2001.
- /2/ Steinbrück, M., Homann, C., Miassoedov, A., Schanz, G., Sepold, L., Stegmaier, U., Steiner, H.: Results of the B₄C Control Rod Test QUENCH-07, FZKA 6746, to be published.
- /3/ Sepold, L., Krauss, W., Miassoedov, A., Steinbrück, M., Stuckert, J.: QUENCH-09 Quick Look Report, SAM-COLOSS-P041, Karlsruhe, Nov. 2002.
- /4/ Miassoedov, A.: Minutes of the COLOSS Topical Meeting on QUENCH-07 Test, SAM-COLOSS-M006, Karlsruhe, Feb. 8, 2001.
- /5/ Homann, Ch., Hering, W., Birchley, J., Fernandez Benitez, J. A., Ortega Bernardo, M.: Analytical Support for B₄C Control Rod Test QUENCH-07, FZKA 6822, SAM-COLOSS-P055, to be published.
- /6/ The SCDAP/RELAP5 Development Team: SCDAP/RELAP5/MOD 3.2 Code Manual, NUREG/CR-6150, INEL-96/0422, Idaho Fall, Idaho, USA, 1997.
- /7/ Hering, W., Homann, C.: Improvement of the Severe Accident Code SCDAP/RELAP5 mod 3.2 with respect to the FZK QUENCH facility, FZKA 6566, to be published.
- /8/ Hering, W., Homann, Ch., Lamy, J.-S., Miassoedov, A., Schanz, G., Steinbrück, M., Sepold, L.: Comparison and Interpretation Report of the OECD International Standard Problem No. 45 Exercise (QUENCH-06), FZKA 6722, July 2002.
- /9/ Miassoedov, A.: Minutes of the COLOSS Topical Meeting on QUENCH-09 and CODEX-B4C Experiments, SAM-COLOSS-M009, Karlsruhe, 22 and 23 Oct. 2002.
- /10/ Duriez, Ch, Adroguer, B.: Minutes of the 4th Progress Meeting, SAM-COLOSS-M011, Bologna, January 31, 2002.
- /11/ Sanchez, V., Elias, E., Homann, Ch., Hering, W., Struwe, D.: Development and Validation of a Transition Boiling Model for the RELAP5/MOD3 Reflood Simulation, FZKA 5954, Sep. 1997.
- /12/ Hofmann, P., Hering, W., Homann, C., Leiling, W., Miassoedov, A., Piel, D., Schmidt, L., Sepold, L., Steinbrück, M.: QUENCH-01 Experimental and Calculational Results, FZKA 6100, Nov. 1998.
- /13/ Hofmann, P., Homann, C., Leiling, W., Miassoedov, A., Piel, D., Schanz, G., Schmidt, L., Sepold, L., Steinbrück, M.: Experimental and Calculational Results of the experiments QUENCH-02 and QUENCH-03, FZKA 6295, July 2000.

Figures

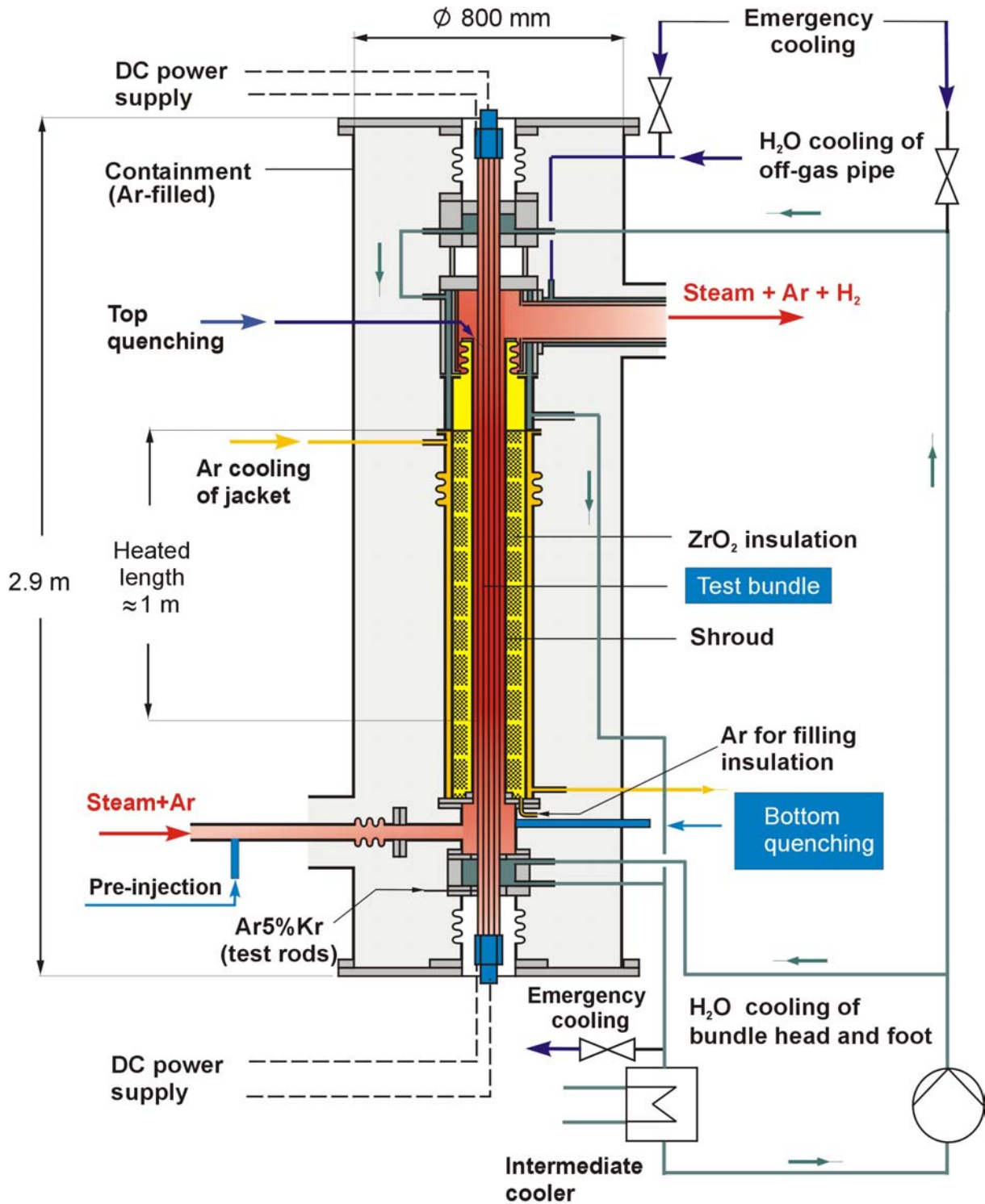


Fig 4 QUE07 Flow lines (ab QUE05).cdr
17.07.02 - IMF

Fig. 1: Main flow paths in the QUENCH facility

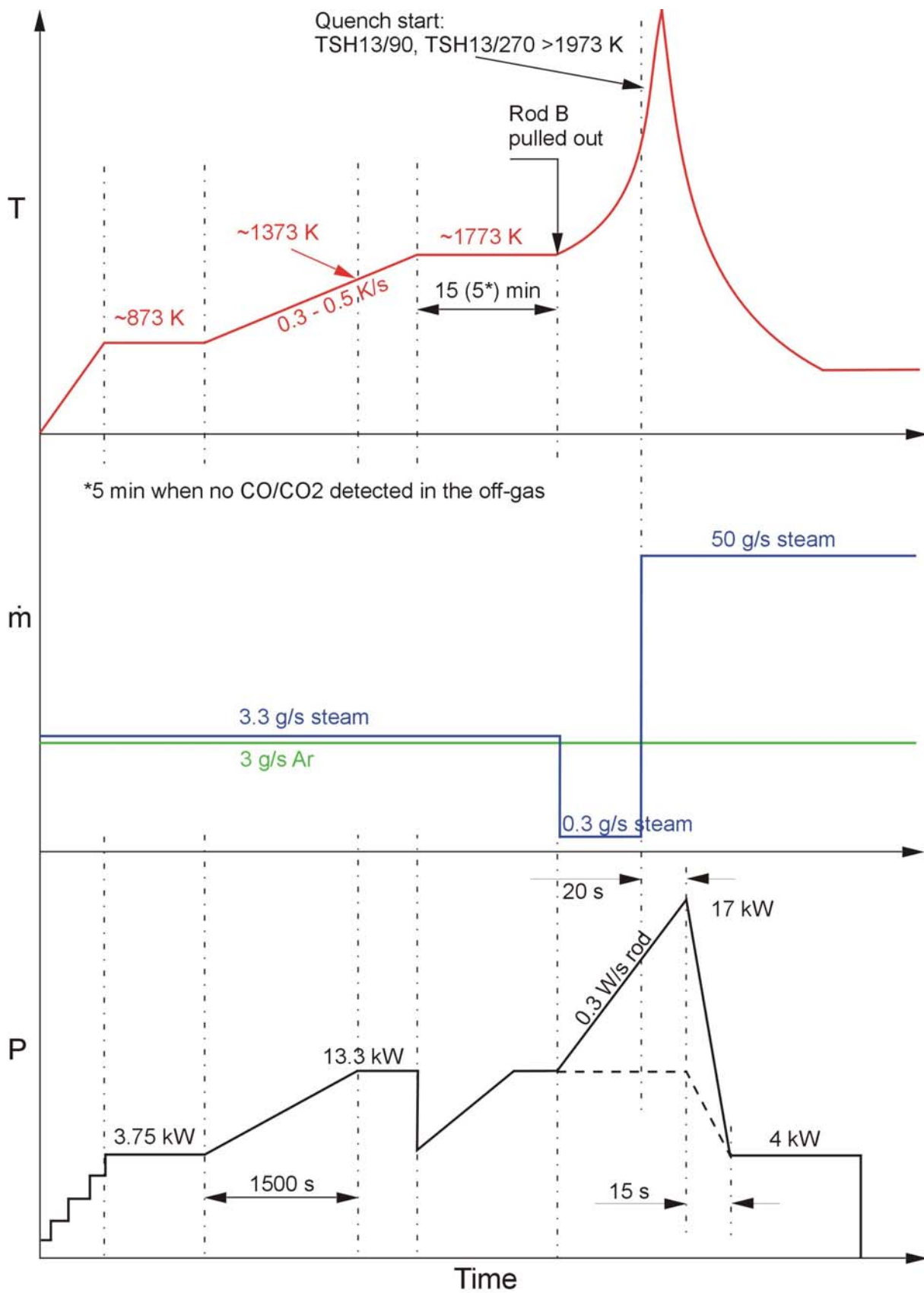


Fig.16-QUE09-performance as planned.cdr
12.08.02 - IMF

Fig. 3: Test protocol for QUENCH-09

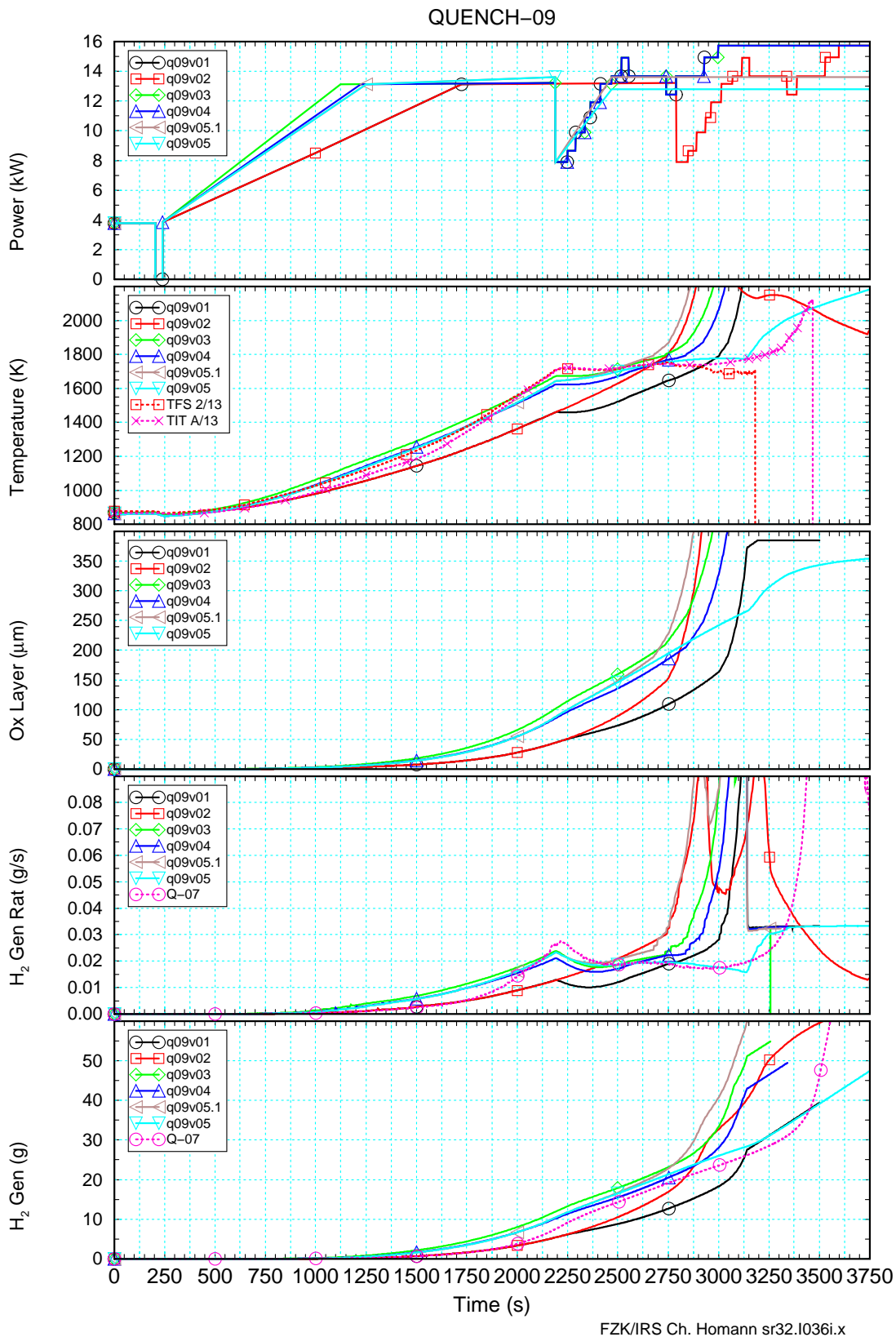


Fig. 5: Survey of pre-test calculations with 16f model

The figure shows from top to bottom electrical power input, temperatures and oxide layer thickness at axial level 13 (elevation 0.05 m), hydrogen production rate, and cumulated hydrogen mass. In the legends experimental values (TFS 2/13, TIT A/13, and Q-07) refer to QUENCH-07, the other labels refer to identifiers for the computational runs.

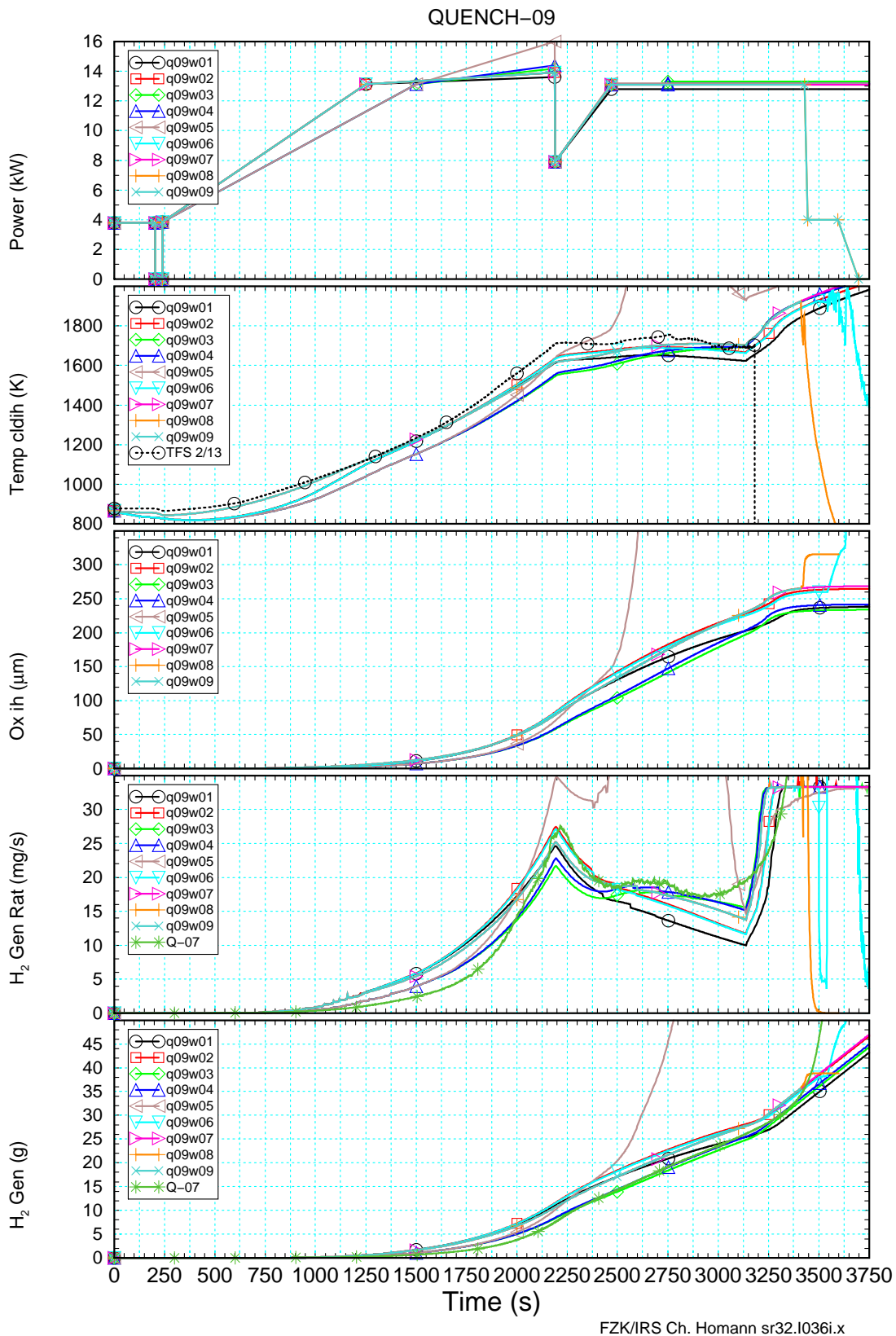


Fig. 6: Survey of pre-test calculations with 32f model

The figure shows from top to bottom electrical power input, temperatures and oxide layer thickness at axial level 13 (elevation 0.95 m), hydrogen production rate, and cumulated hydrogen mass. In the legends experimental values (TFS 2/13, TIT A/13, and Q-07) refer to QUENCH-07, the other labels refer to identifiers for the computational runs.

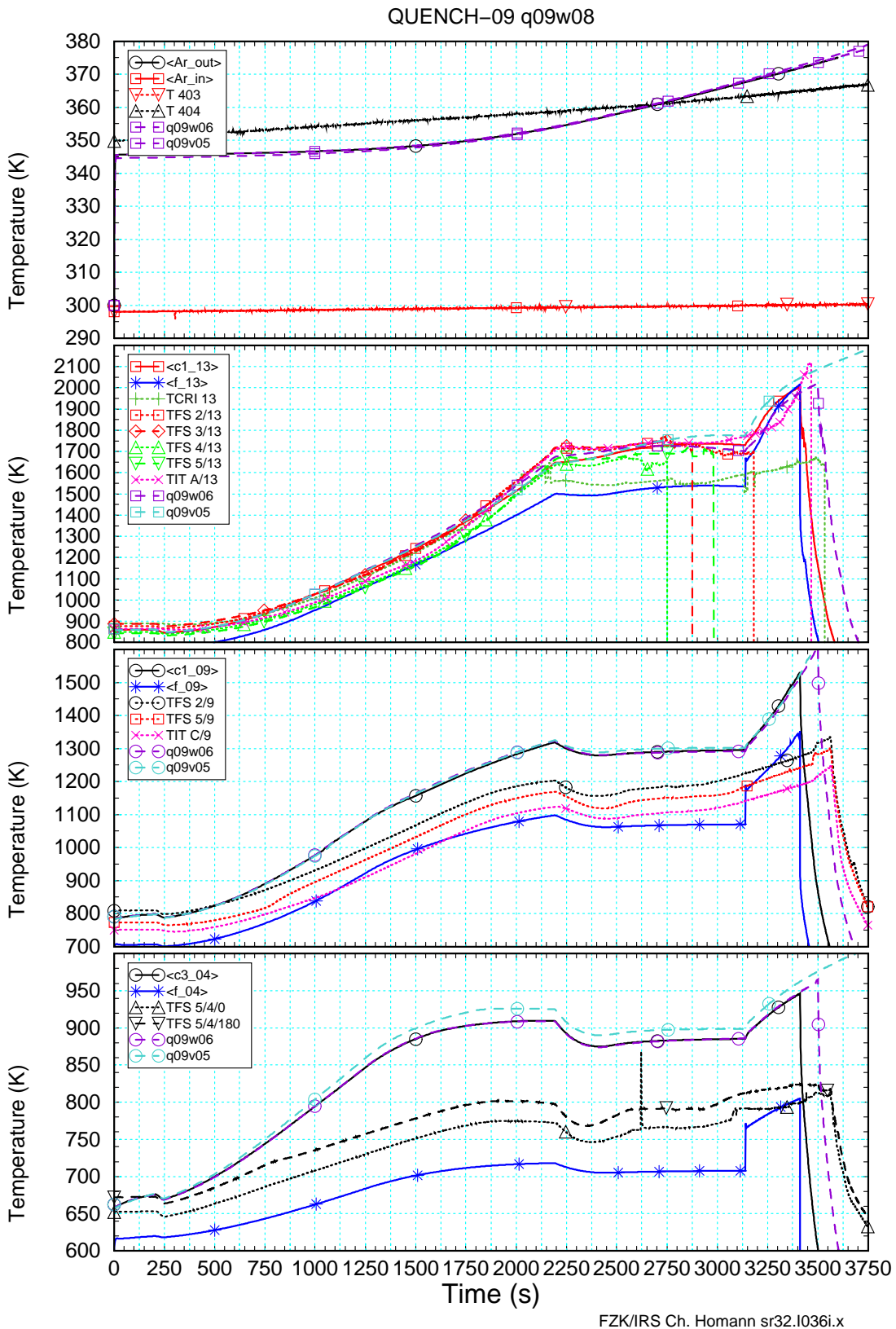
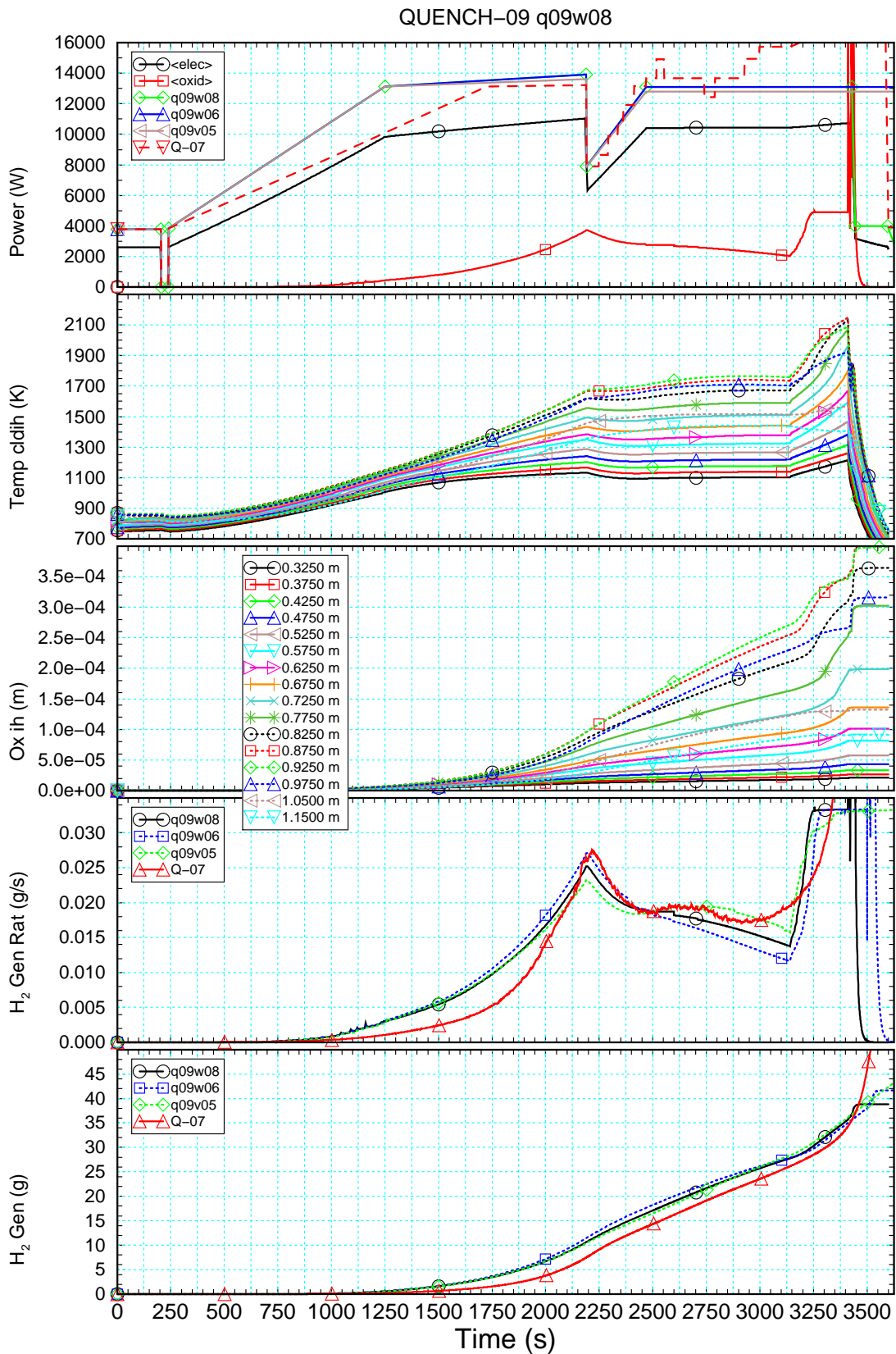


Fig. 7: Temperatures as a function of time (pre-test calculations)

The figure shows from top to bottom inlet and outlet temperatures in the argon cooling and clad temperatures for the inner heated rods at axial levels 13, 9, and 4 (elevations 0.95, 0.55, and 0.05 m).



FZK/IRS Ch. Homann sr32.i036i.x

Fig. 8: Selected variables as a function of time (pre-test calculations)

The figure shows from top to bottom electrical and chemical power released in the bundle, temperatures and oxide layer thickness for the inner heated rods, hydrogen production rate, and cumulated hydrogen mass.

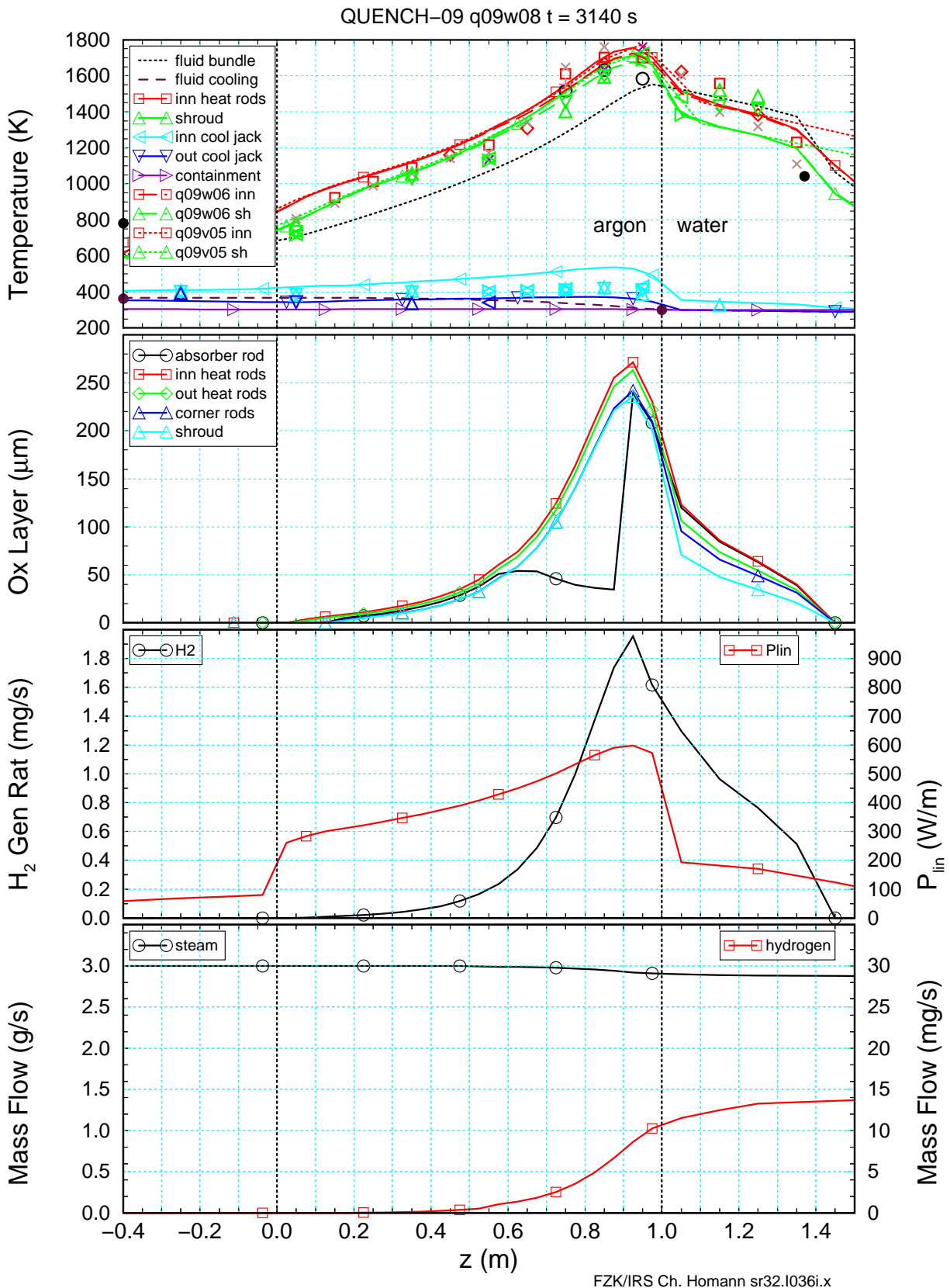


Fig. 9: Axial profiles of selected variables, part 1 (pre-test calculations)

The figure shows from top to bottom temperatures, oxide layer thickness, hydrogen production rate, linear electrical rod power, steam, and hydrogen mass flow rates at the end of the plateau phase.

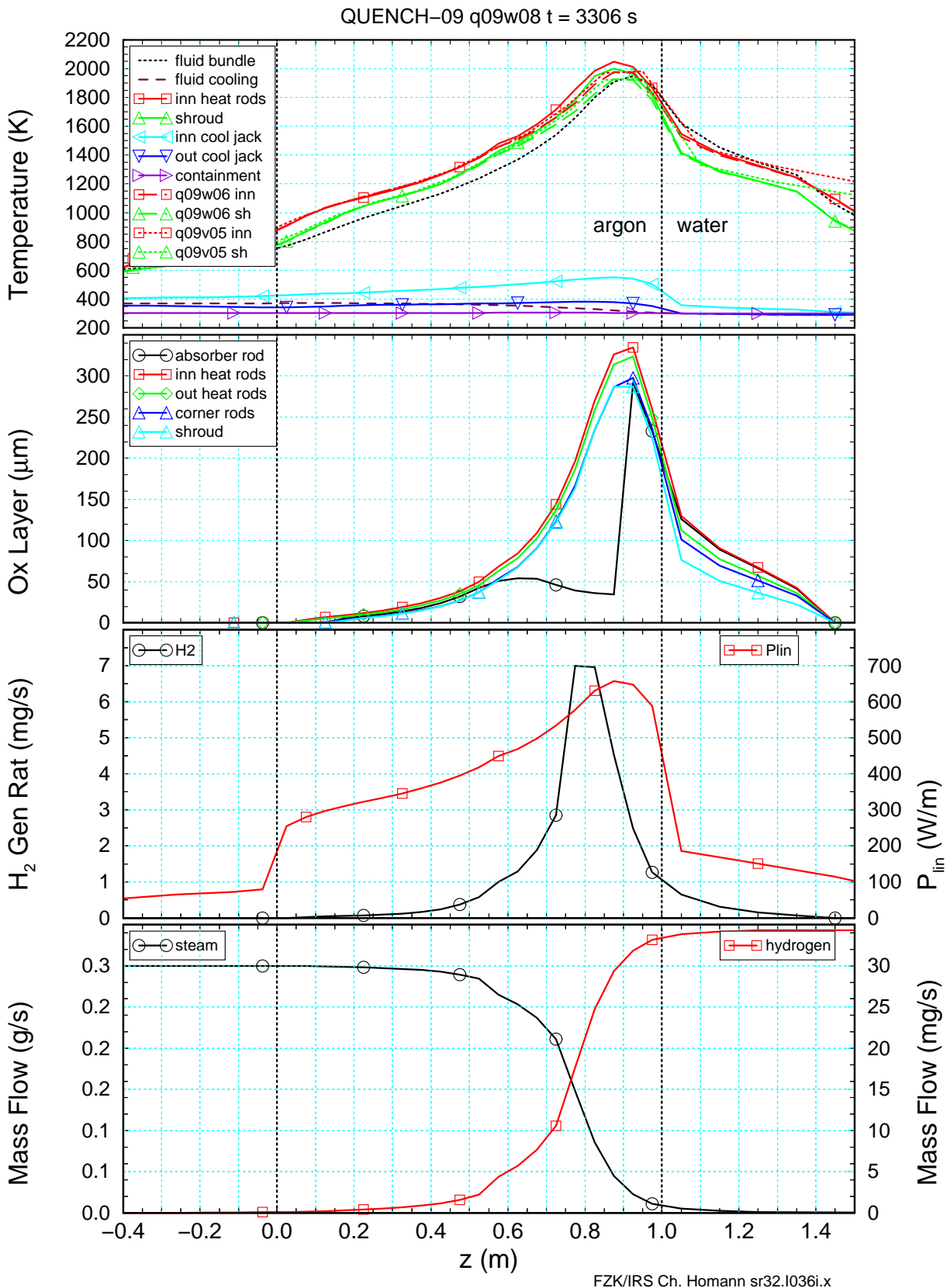


Fig. 10: Axial profiles of selected variables, part 2 (pre-test calculations)

The figure shows from top to bottom temperatures, oxide layer thickness, hydrogen production rate, linear electrical rod power, steam, and hydrogen mass flow rates during the second transient.

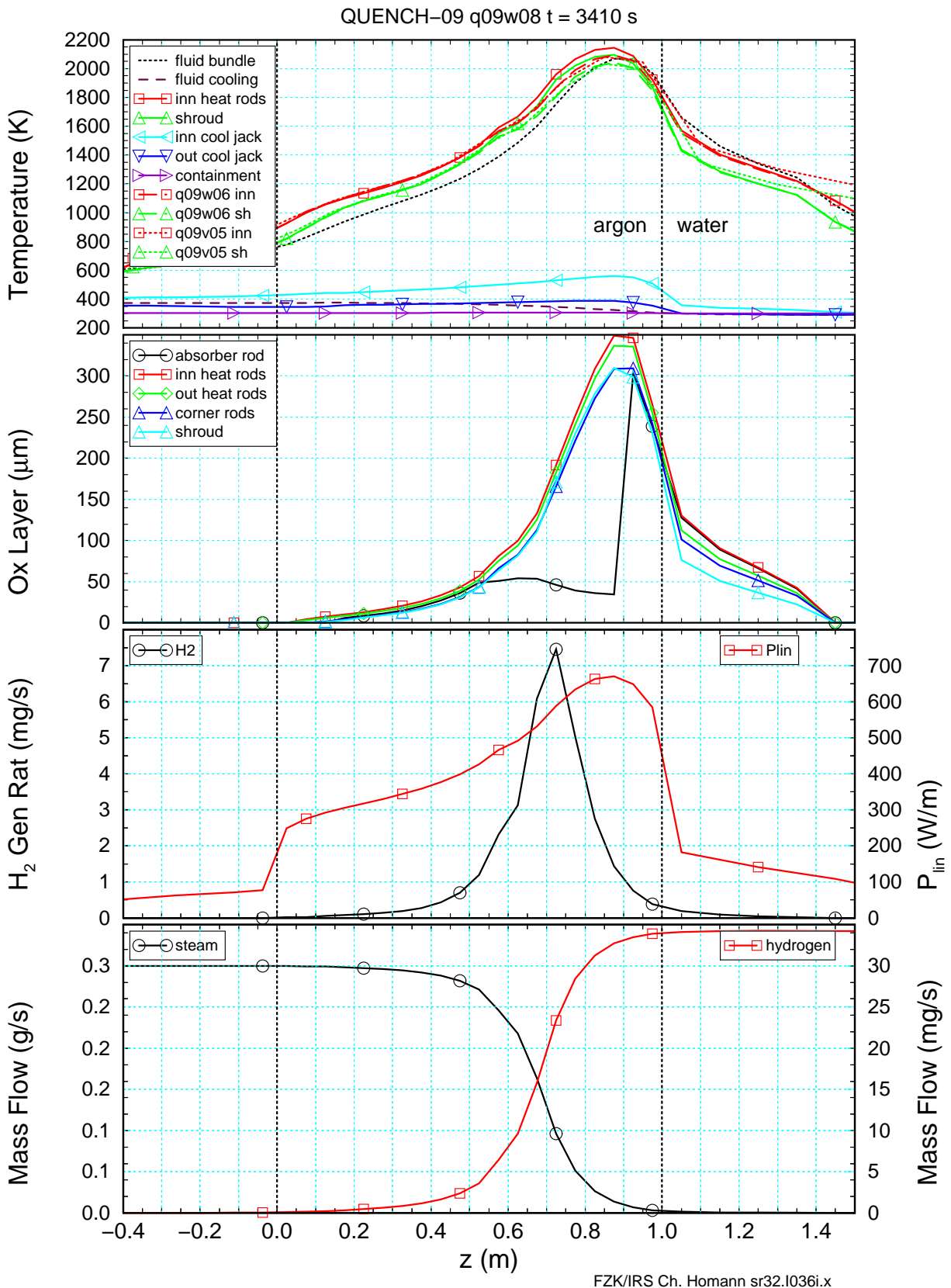


Fig. 11: Axial profiles of selected variables, part 3 (pre-test calculations)

The figure shows from top to bottom temperatures, oxide layer thickness, hydrogen production rate, linear electrical rod power, steam, and hydrogen mass flow rates at the end of the second transient.

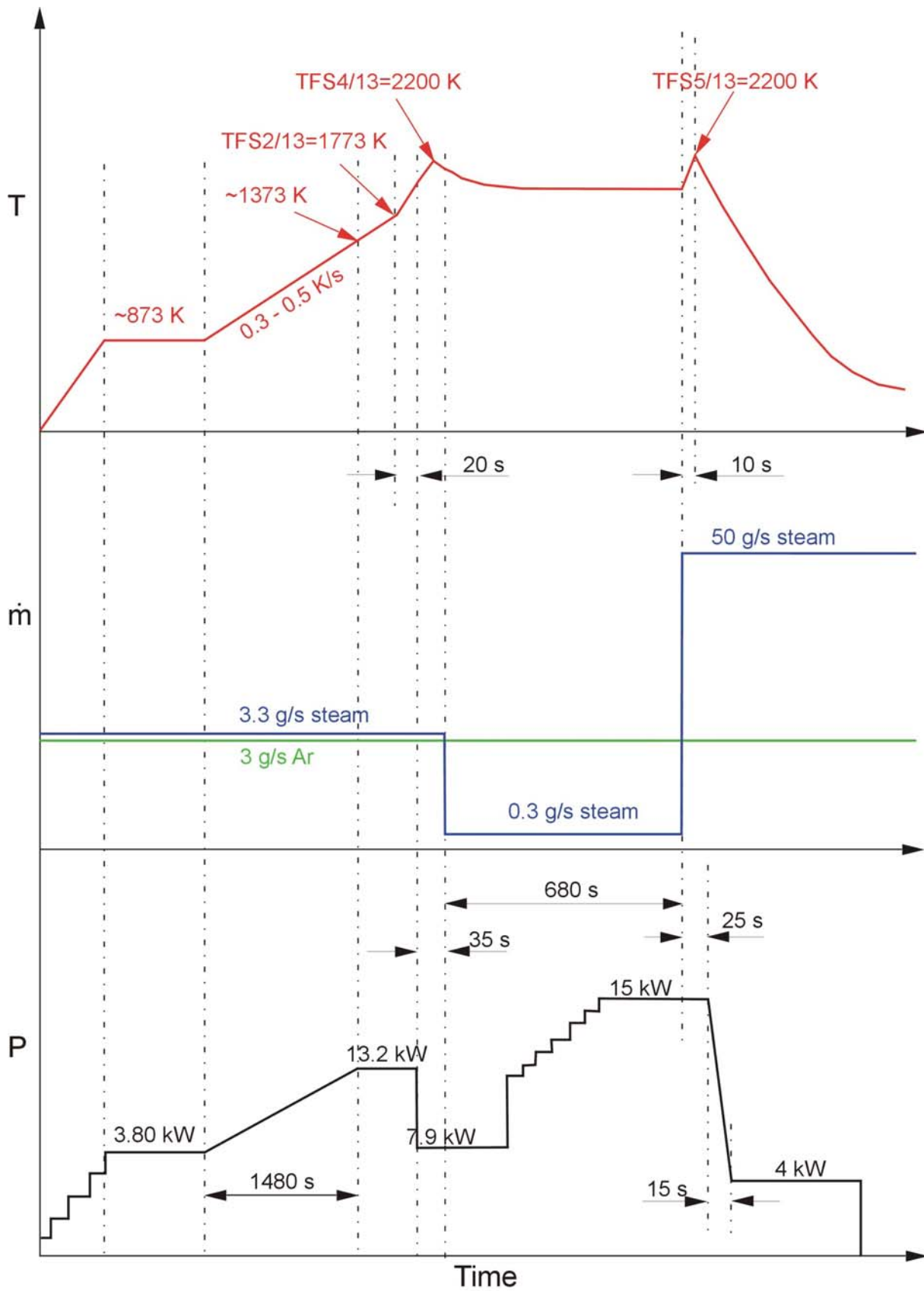
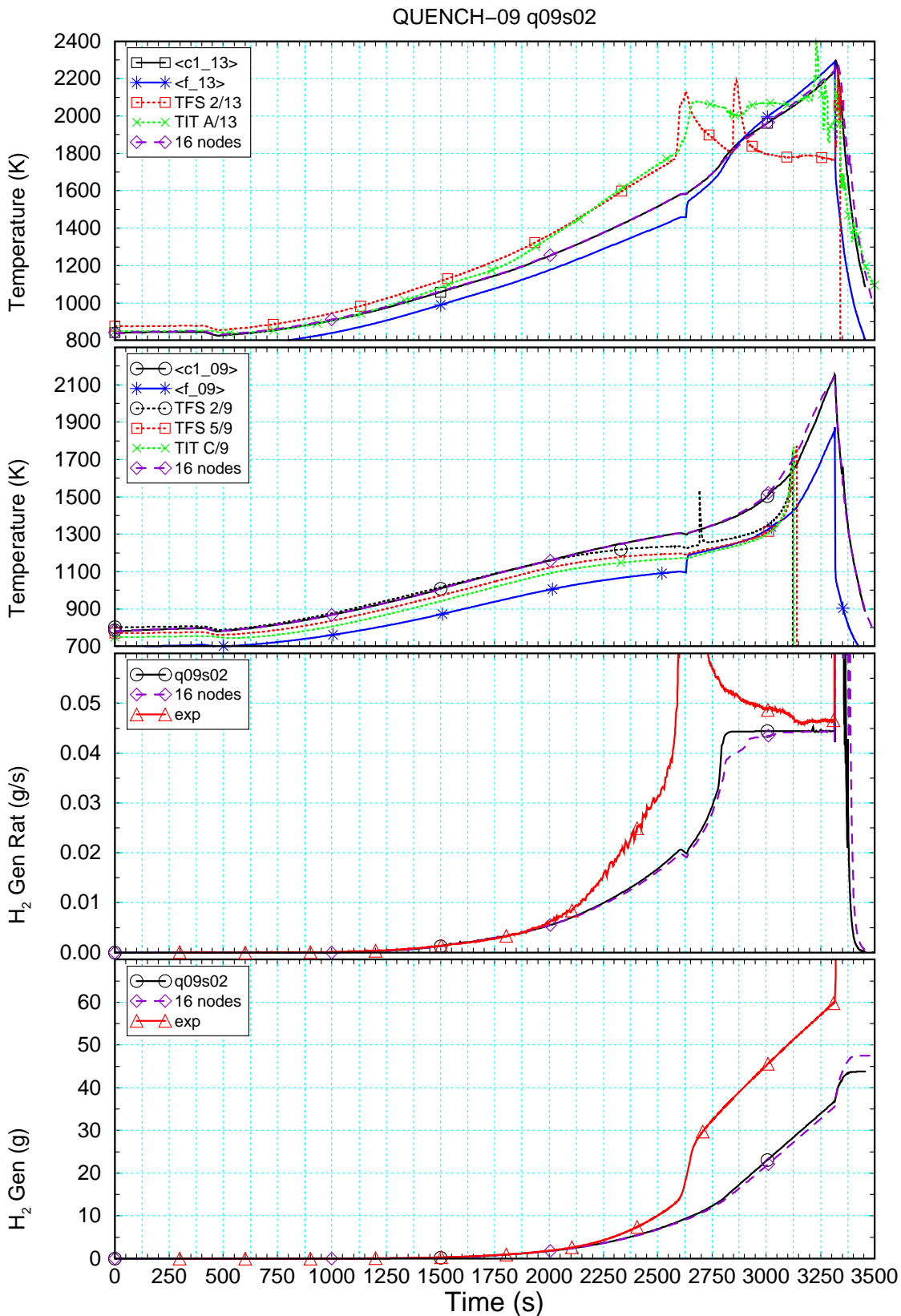


Fig.17-QUE09-as performed.cdr
12.08.02 - IMF

Fig. 12: Conduct of test QUENCH-09



FZK/IRS Ch. Homann sr32.i036j.x

Fig. 13: Selected variables as a function of time (post-test calculation)

The figure shows from top to bottom calculated and measured values for temperatures at axial levels 13 and 9 (elevations 0.95 and 0.55 m), hydrogen production rate, and cumulated hydrogen mass for calculated and measured results.

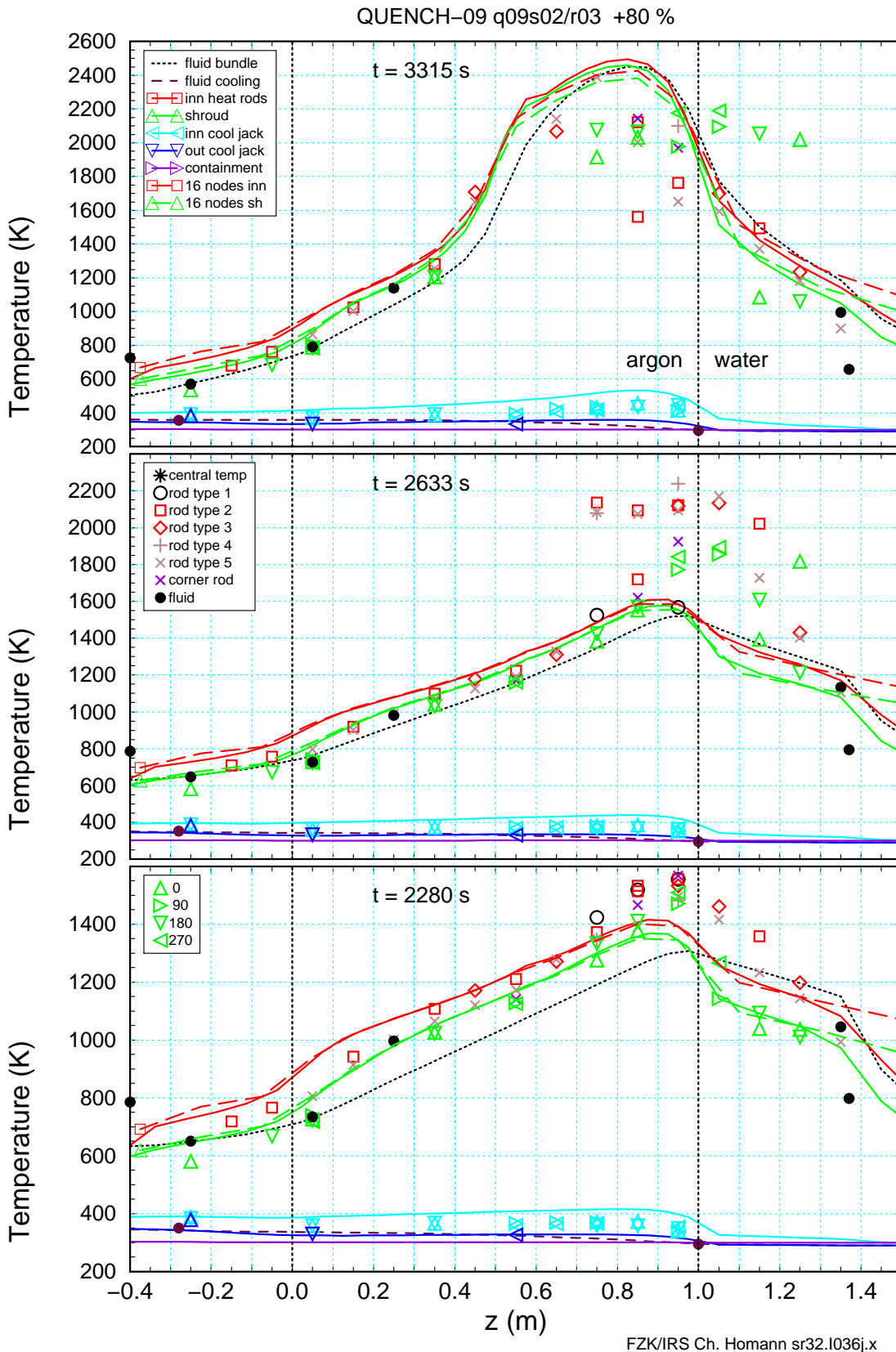
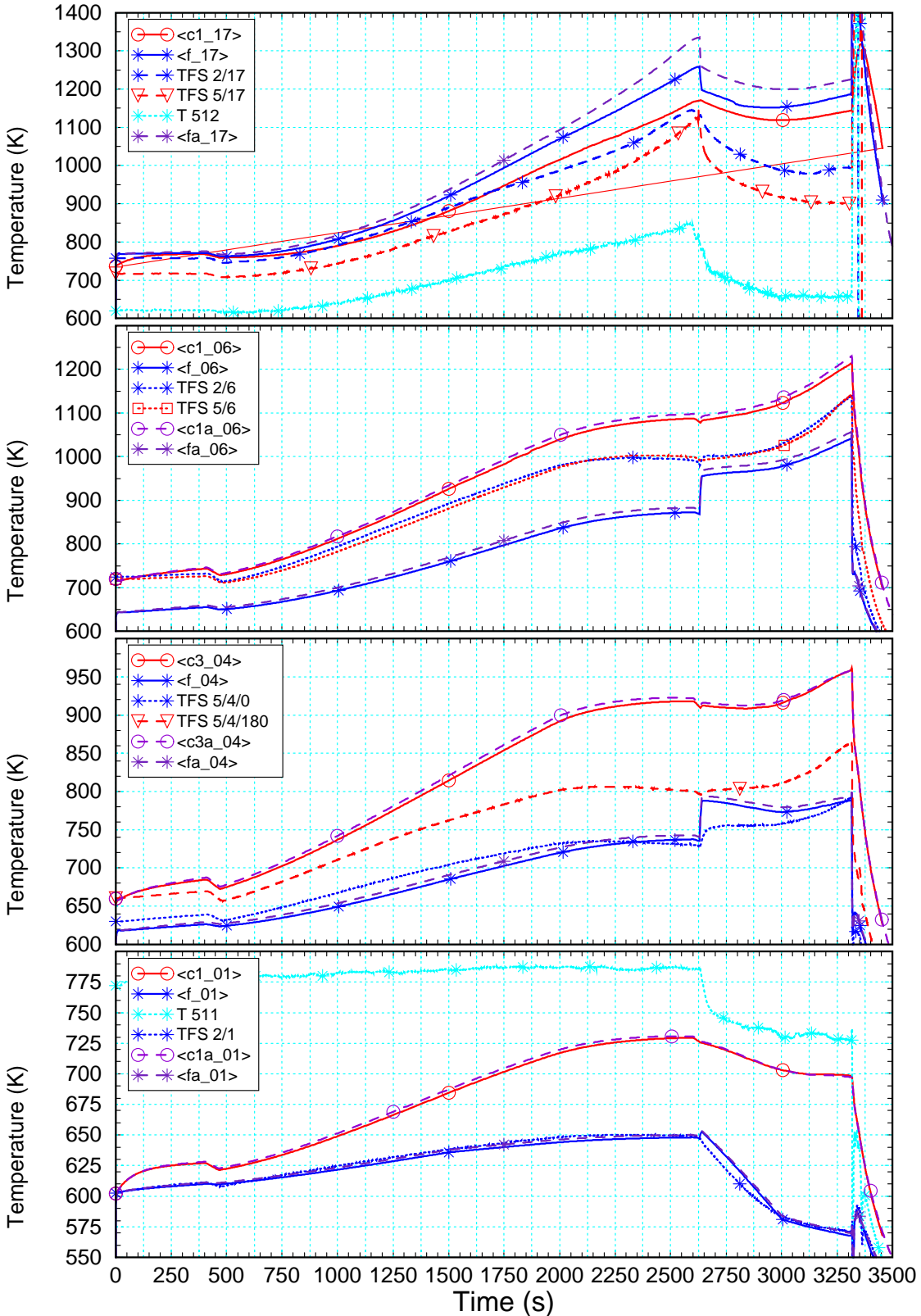


Fig. 14: Axial temperature profiles at three different times (post-test calculation)

The figure shows calculated and measured temperatures for inner heated rods, the shroud, the inner and outer cooling jacket, the containment and for the fluid in bundle and cooling at the beginning of the cool-down phase, at the beginning of steam mass flow reduction, and the time of absorber rod failure (from top to bottom).

QUENCH-09 q09s02/q09s03



FZK/IRS Ch. Homann sr32.i036j.x

Fig. 15: Measured and calculated fluid temperatures (post-test calculation)

The figure shows from top to bottom calculated and measured temperatures at levels 17, 6, 4, and 1 (elevations 1.35, 0.25, 0.05, and -0.25 m).

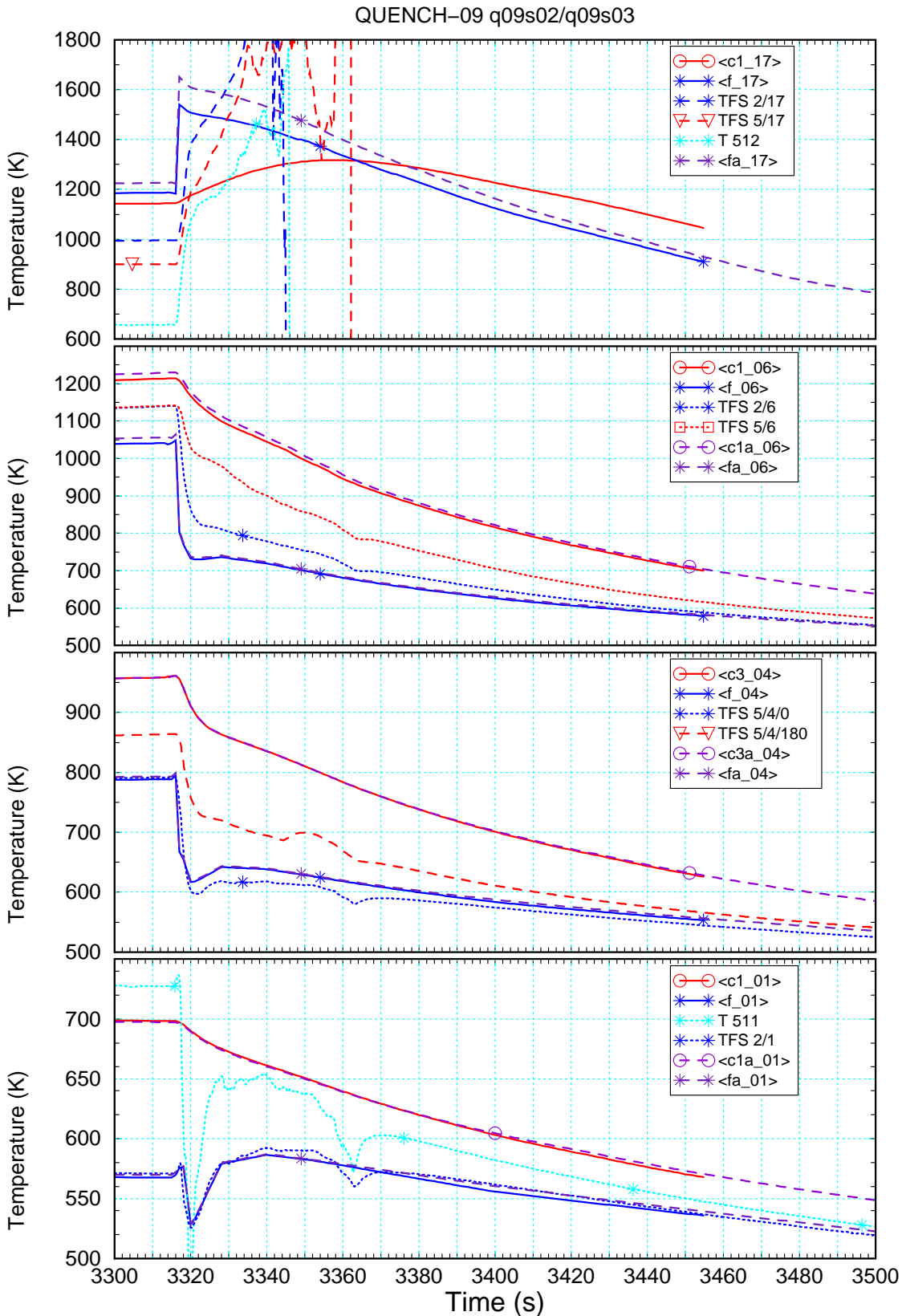
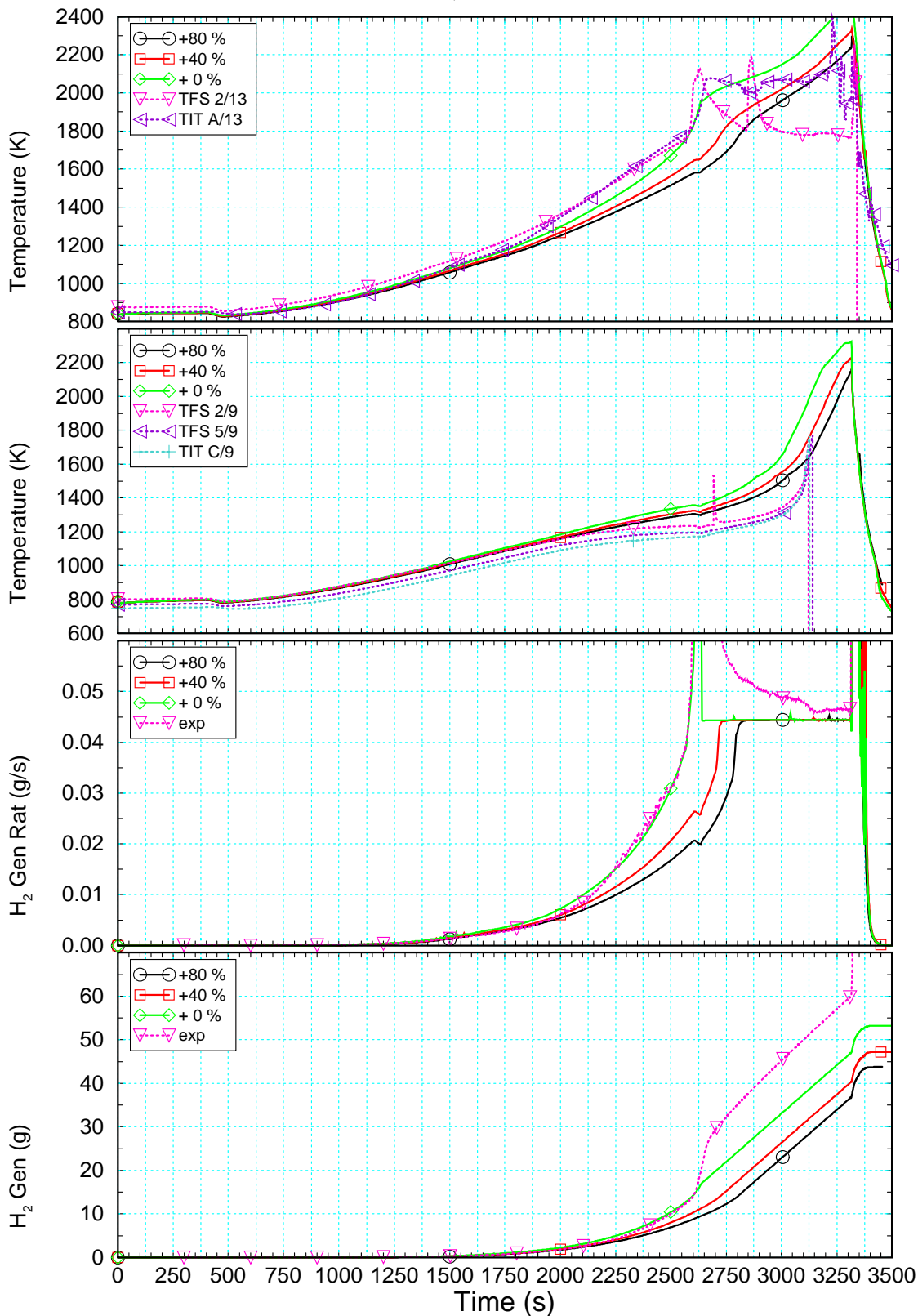


Fig. 16: Measured and calculated fluid temperatures (post-test calculation, cool-down)

The figure shows from top to bottom calculated and measured temperatures at levels 17, 6, 4, and 1 (elevations 1.35, 0.25, 0.05, and -0.25 m).

QUENCH-09



FZK/IRS Ch. Homann sr32.i036j.x

Fig. 17: Selected variables as a function of time (parameter study)

The figure shows from top to bottom calculated and measured temperatures at axial levels 13 and 9 (elevations 0.95 and 0.55 m), hydrogen production rate, and cumulated hydrogen mass for the three increases (80, 40, and 0 %, respectively) of thermal conductivity of shroud insulation with respect to manufacturer's data.

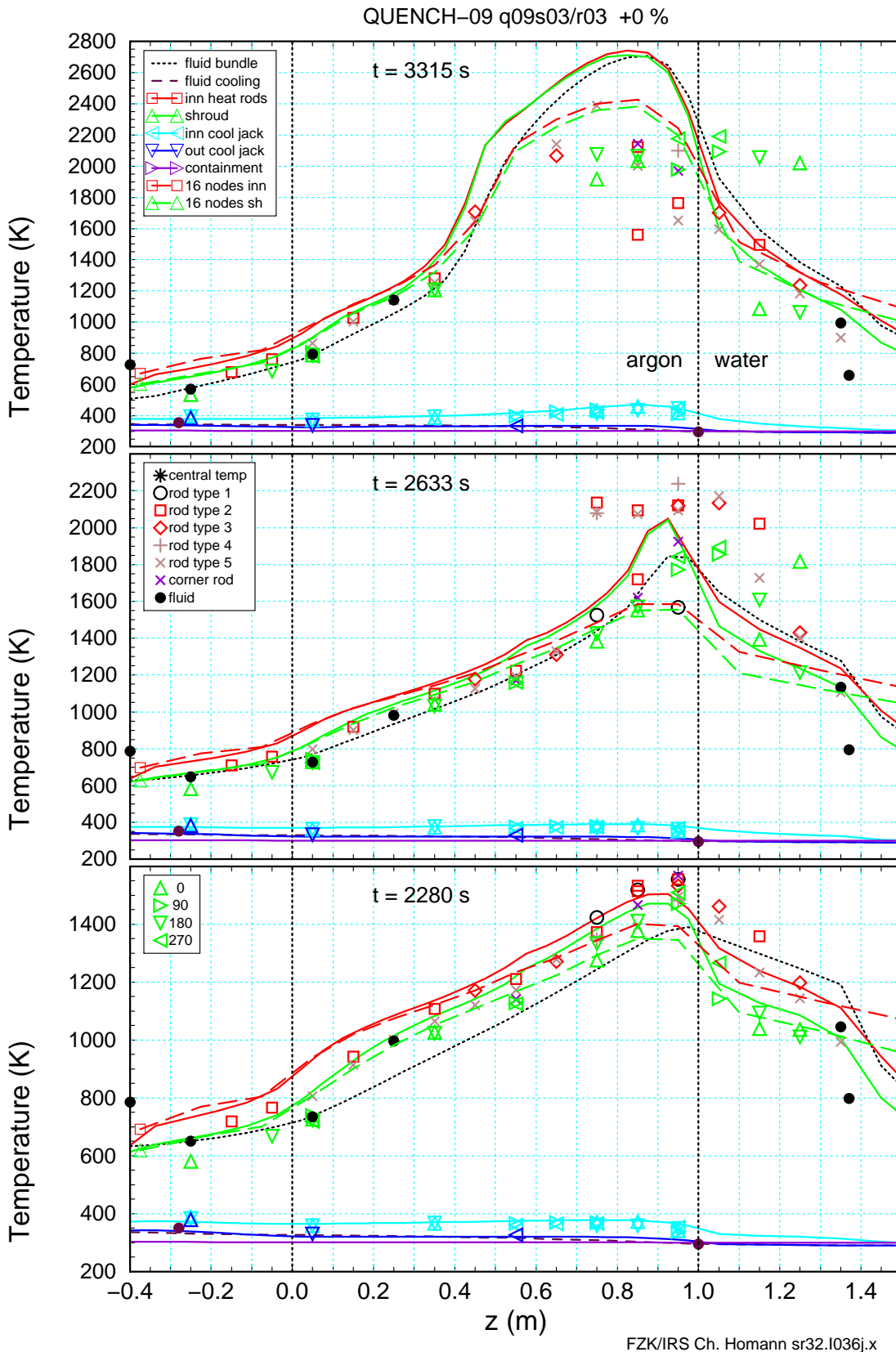


Fig. 18: Axial temperature profiles (manufacturer's data for shroud insulation)

The figure shows calculated and measured temperatures for inner heated rods, the shroud, the inner and outer cooling jacket, the containment and for the fluid in bundle and cooling at the beginning of the cool-down phase, at the beginning of steam mass flow reduction, and at the time of absorber rod failure (from top to bottom).

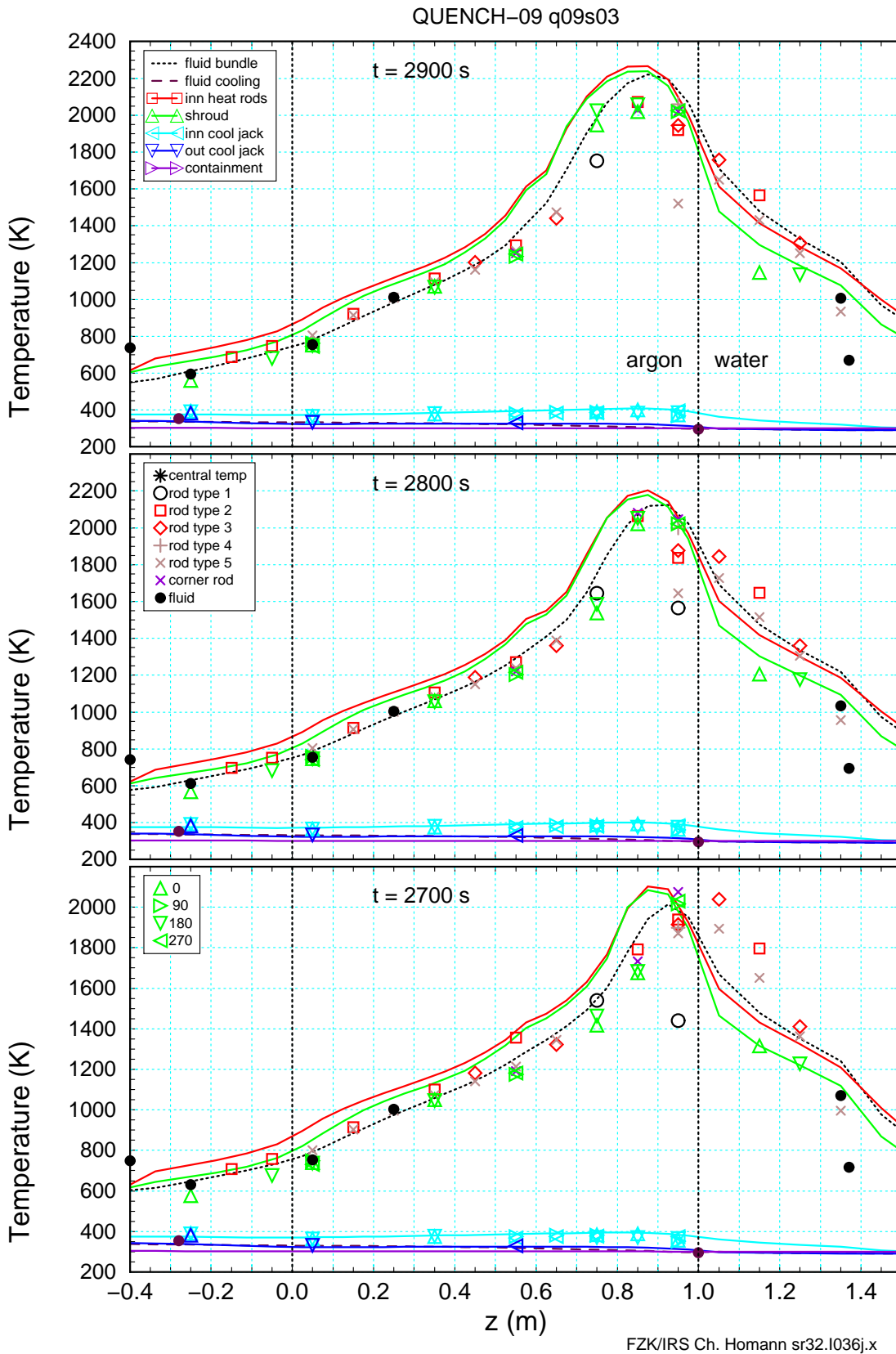


Fig. 19: Axial temperature profiles in the second transient (part 1)

The figure shows calculated and measured temperatures for inner heated rods, the shroud, inner and outer cooling jacket, the containment and for the fluid in bundle and cooling at three times during the second transient. Manufacturer's data for shroud insulation are used in the calculation.

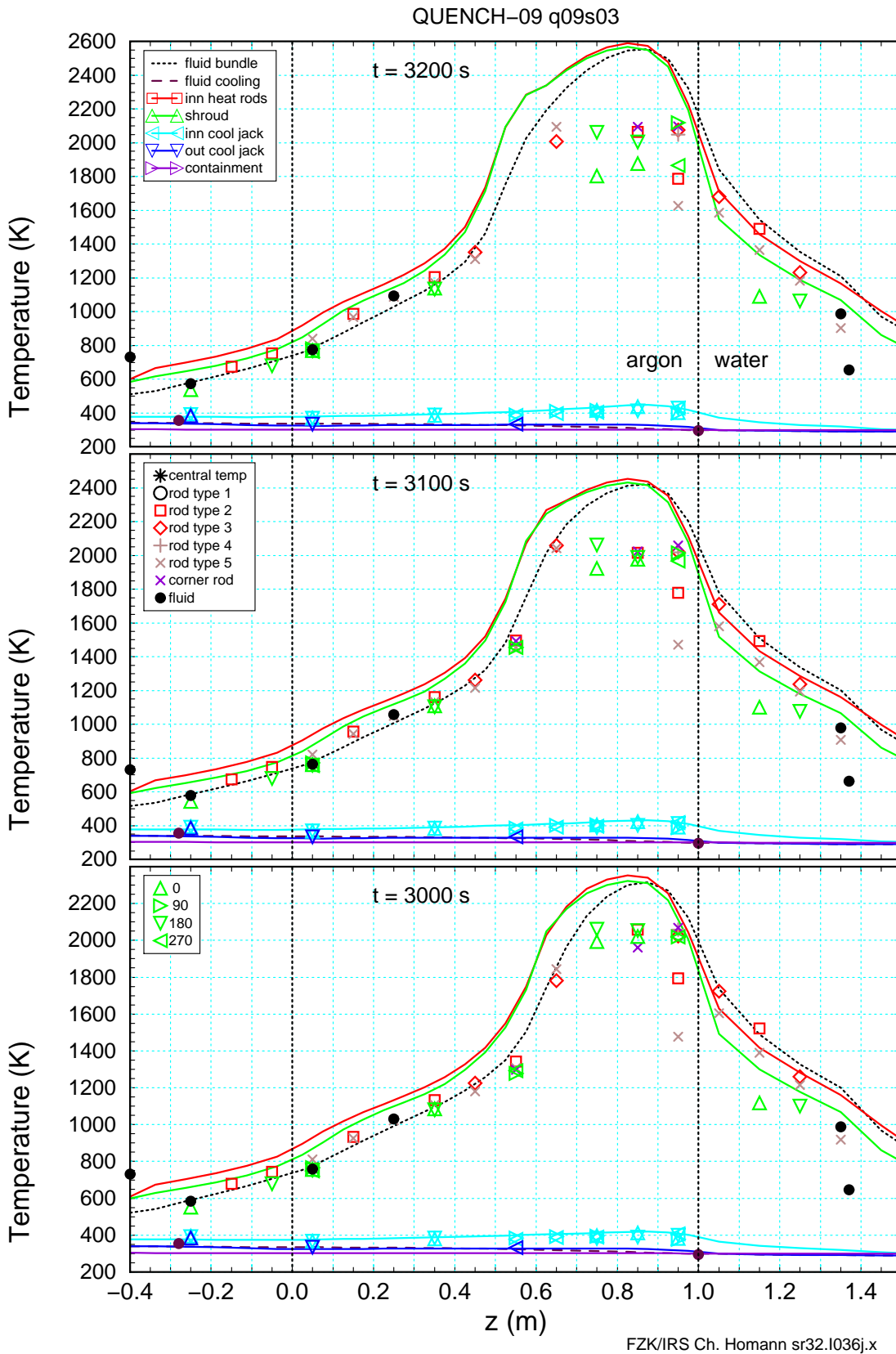
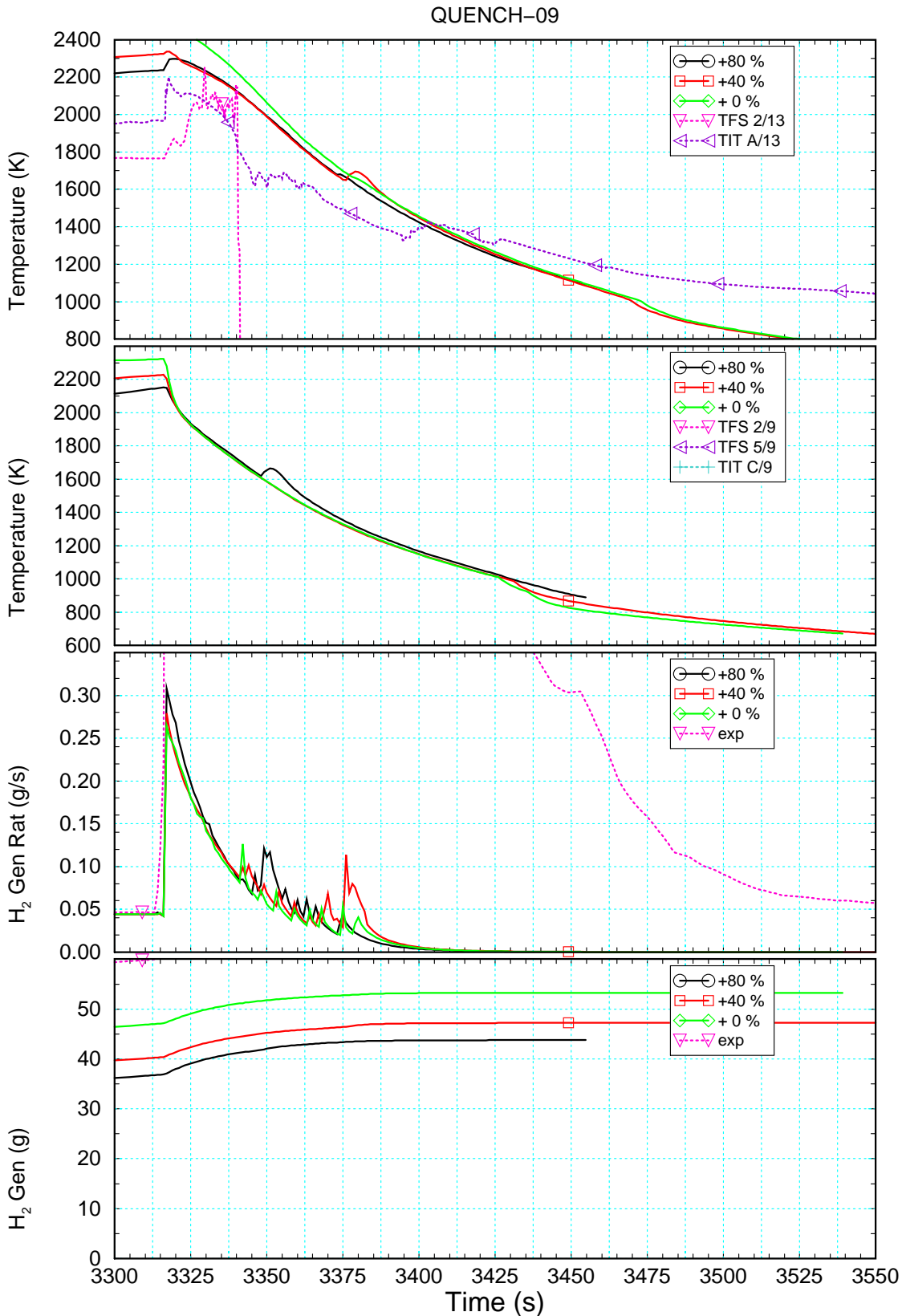


Fig. 20: Axial temperature profiles in the second transient (part 2)

The figure shows calculated and measured temperatures for inner heated rods, the shroud, inner and outer cooling jacket, the containment and for the fluid in bundle and cooling at three times during the second transient. Manufacturer's data for shroud insulation are used in the calculation.

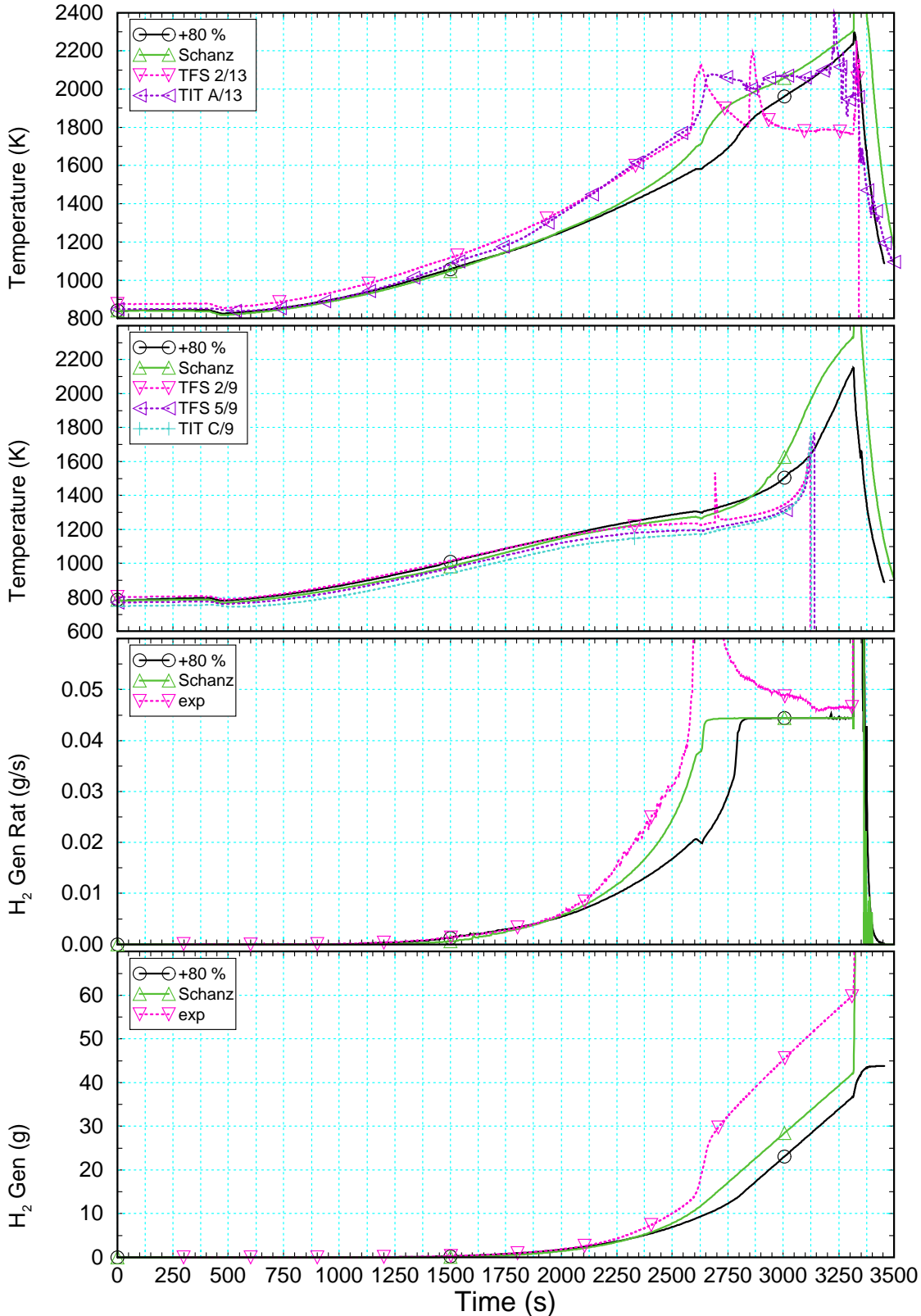


FZK/IRS Ch. Homann sr32.i036j.x

Fig. 21: Selected variables as a function of time (parameter study, cool-down phase)

The figure shows from top to bottom calculated and measured temperatures at axial levels 13 and 9 (elevations 0.95 and 0.55 m), hydrogen production rate, and cumulated hydrogen mass for the three increases (80, 40, and 0 %, respectively) of thermal conductivity of shroud insulation with respect to manufacturer's data.

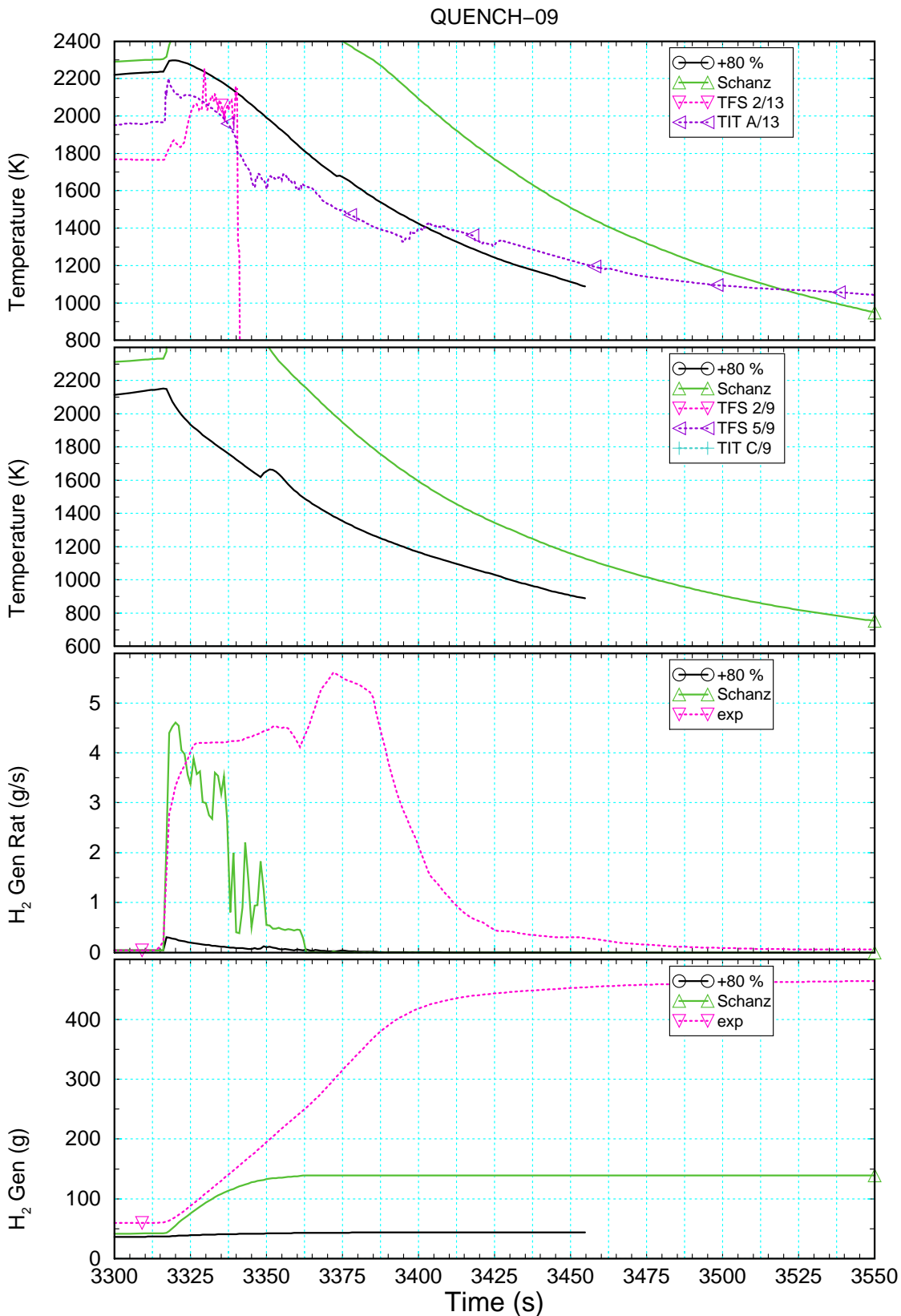
QUENCH-09



FZK/IRS Ch. Homann sr32.i036j.x

Fig. 22: Selected variables as a function of time (oxidation correlation)

The figure shows from top to bottom calculated and measured temperatures at axial levels 13 and 9 (elevations 0.95 and 0.55 m), hydrogen production rate, and cumulated hydrogen mass for the standard (label "+80 %") and the oxidation correlation recommended in COLOSS (label "Schanz").



FZK/IRS Ch. Homann sr32.i036j.x

Fig. 23: Selected variables as a function of time (oxidation correlation, cool-down phase)

The figure shows from top to bottom calculated and measured temperatures at axial levels 13 and 9 (elevations 0.95 and 0.55 m), hydrogen production rate, and cumulated hydrogen mass for the standard (label “+80 %”) and the oxidation correlation recommended in COLOSS (label “Schanz”).